CHAPTER 3

Basaltic lava domes, lava lakes, and volcanic segmentation on the southern East Pacific Rise

Abstract. Meter-scale DSL-120 sonar mapping and coregistered *Argo II* photographic observations reveal changes in eruptive style that closely follow the third-order structural segmentation of the ridge axis on the southern East Pacific Rise, 17°11'-18°37'S. Near segment ends we observe abundant basaltic lava domes which average 20 m in height and 200 m in basal diameter and have pillow lava as the dominant lava morphology. The ubiquity of pillow lava suggests low effusion rate eruptions. The abundance of lava domes suggests that the fissure eruptions were of sufficient duration to focus and produce a line of volcanic edifices. Near segment centers we observe fewer but larger lava domes, voluminous drained and collapsed lava lakes, and smooth lobate and sheet lava flows with very little pillow lava. The abundance of sheet flows suggests that high effusion rate eruptions are common. Fewer lava domes and large lava lakes suggest that fissure eruptions do not focus to point sources. This pattern was observed on eight third-order ridge segments suggesting that a fundamental volcanic segmentation of the ridge occurs on this scale. The third-order segment boundaries also correlate with local maxima in the seismic axial magma chamber reflector depth throughout the study area and decreased across-axis width of the region of seismic layer 2A thickening along the one segment where sufficient cross-axis seismic lines exist. The geochemically defined magmatic segment boundaries in the study area match the locations of our volcanic segment boundaries, although rock sampling density is not adequate to constrain the variation across all the third-order volcanic segments that we identify. These observations suggest that variation in the processes of crustal accretion along axis occurs at a length scale of tens of kilometers on superfast spreading (>140 km/Myr full rate) mid-ocean ridges.

1. Introduction

The spreading axis of the mid-ocean ridge is interrupted at many length scales by morphologic ridge axis discontinuities (RADs) that divide the ridge into structural segments. Individual structural segments often have a geochemistry or tectonic history distinctive from their neighbors [see *Batiza*, 1996; *Macdonald*, 1998, and references therein]. As seafloor maps are made at higher levels of resolution and with more complete spatial coverage, progressively finer scales of segmentation become apparent. Classification of segments based on segment length, RAD offset size,

geochemical variations, and longevity of segments and their bounding RADs permit the recognition of similar orders of segmentation on different ridges [*Langmuir et al.,* 1986; *Macdonald et al.,* 1988, 1991]. Yet the origins of these scales of ridge segmentation remain elusive.

In this paper, we focus on a level of segmentation that operates on a smaller scale than the segments defined by transform faults (first-order), or by large overlapping spreading centers (OSCs) and propagating rifts (second-order, see Table 1). The discontinuities which define this finer scale of segmentation are typically very small OSCs (offsets less than ~1 km), local topographic lows or saddle points, and intersections of neighboring segments which have slightly different strikes (deviations from axial linearity (Devals)). These are the smallest RADs that are easily detectable using hull-mounted multibeam echosounders. Off-axis discordant zones associated with these discontinuities are either very small or undetectable, so it is inferred that the intervening segments are short-lived (10^3-10^5 years) [*Macdonald et al.,* 1988]. These third-order segments are typically ten to a few tens of kilometers long. An even finer scale of segmentation (fourth-order), defined by even smaller RADs, can be resolved with near-bottom sensors or fine-scale rock sampling [e.g., *Langmuir et al.,* 1986; *Macdonald et al.,* 1988].

Many lines of evidence point to a segmented volcanic plumbing system beneath fast spreading ridges, but details of the segmentation are unknown owing to the lack of information about the eruptive history of the ridge. Seismic investigations along the southern East Pacific Rise (SEPR) show that a phase-reversed reflector, apparently produced at the roof of the Axial Magma Chamber (AMC), is present under most of the ridge, except at OSCs [*Detrick et al.,* 1993]. Even where the AMC reflector is continuous, the AMC itself may be segmented into discrete melt pockets separated by zones of crystalline mush [*Singh et al.,* 1998]. Seismic refraction studies suggest that the crust is thicker and forms over a narrower zone around ridge offsets than near midsegment on superfast and fast spreading ridges [*Barth and Mutter,* 1996; *Hooft et al.,* 1997; *Carbotte et al.,* 1997; *Canales et al.,* 1998]. Geochemical analyses of closely spaced (<10 km) rock samples show variations in lava composition correlating with second- or third-order structural segments on the EPR [*Langmuir et al.,* 1986; *Sinton et al.,* 1991; *Reynolds et al.,* 1992]. Merging our fine-scale observations of eruptive styles on the SEPR with the insights provided by previous seismic and geochemical studies permits us to develop a new model for the significance of third-order ridge segments as individual volcanic systems along the superfast spreading ridge axis.

Published lava morphology data from mapping of fast to superfast spreading ridges indicate that the lava morphology is dominated by sheet flows generated by fissure eruptions [*Renard et al.*, 1985; *Gente et al.*, 1986; *Haymon et al.*, 1993; *Auzende et al.*, 1996; *Fornari et al.*, 1998]. However, the vast majority of this mapping is from locally detailed but spatially limited submersible observations concentrated toward the middle of magmatically robust ridge segments. From these observations the belief arose that fast spreading ridges mainly erupt sheet flows and very little pillow lava [*Bonatti and Harrison*, 1988; *Perfit and Chadwick*, 1998]. One exception to these spatially limited observations is an *Argo* survey of the northern EPR (9°09'-9°54'N) that covered 83 km of the ridge crest (including all but the ends of a second-order ridge segment) and found lobate flows associated with large collapsed lava lakes [*Haymon et al.*, 1991]. Sheet flow eruptions should produce thin lava flows with little to no relief, creating no volcanic constructions. However, our extensive 1996 survey of the superfast spreading SEPR provides new evidence that outside of limited regions of collapsed lava lakes, dome-shaped mounds of pillow lava are the most common volcanic structure (Figure 1).

We present evidence that third-order RADs are the geomorphic expression of breaks in the volcanic plumbing system of the superfast spreading SEPR. The spatial distribution of volcanic structures, primarily the contrast between small dome-shaped pillow mounds near third-order RADs and extensive collapses of hollow lobate and sheet lava flows near segment centers, suggests that third-order RADs are sites of lower effusion rate eruptions than segment centers. The systematic variation from high-to-low effusion rate eruptions on third-order segments suggests that the volcanic systems on superfast spreading ridges are organized at this scale of segmentation.

2. Overview of the Structure of the EPR, 17°11'-18°37'S

The SEPR is currently the fastest spreading mid-ocean ridge [*DeMets et al.*, 1990], opening at rates (~140 mm/yr) close to the fastest documented rate in the geologic record [*Wilson*, 1996]. Accordingly, the SEPR is probably producing the most continuous record of mid-ocean ridge magmatism and volcanism. The spreading center throughout the survey area, 17°11'-18°37'S, is a local topographic high, underlain by a low-density region [*Scheirer et al.*, 1998]. The topographic axial high of the SEPR in the survey area is flanked by low abyssal hills and by numerous small, near-axis, isolated volcanoes and volcano chains [*White et al.*, 1998; *Scheirer et al.*, 1996b]. The survey area has an overall morphology that is typical of fast and superfast spreading ocean ridges [*Lonsdale*,

1989; *Macdonald et al.*, 1992; *Cochran et al.*, 1993; *Scheirer et al.*, 1996a; *Sempere et al.*, 1997] (Figure 1).

Our survey of the SEPR, 17°11'-18°37'S, contains the representative morphologies of fast and superfast spreading ridges: the axial high may be characterized by a smooth dome, half-trough, broad-shallow trough, or deep-narrow trough (Figure 2). From 17°11' to 17°56'S the ridge axis lies along the crest of a domed axial high. From the OSC at 17°56' to the OSC at 18°09'S, the ridge axis lies to the west of a 15-30 m high west facing scarp that has no east-facing conjugate (i.e., half graben). From 18°09' to 18°22'S the ridge axis sits within a broad but shallow trough. From 18°22' to 18°37'S the scarps bounding the trough are higher, and the floor of the trough narrows.

A bathymetric map of this area was made from SeaBeam2000 data collected in 1996 with the ridge axis centered beneath the ship in order to minimize the beam footprint on the ridge crest [*Cormier et al.*, 1996; *Scheirer et al.*, 1998]. The resulting map was nearly artifact-free when gridded at 100 m. We picked the RADs used in this study from this bathymetry (Table 2). Given the resolution of the multibeam data, the locations of the RADs picked in this study are precise to within 500 m, but the nature of the RADs is such that they are best described as zones of offset (Figure 1b). The area of our survey contains two third-order OSCs that offset the ridge in a left step of 1 km and have left a faint trace of rapid southward propagation [*Cormier and Macdonald*, 1994]. In addition to the OSCs, our survey area has four left-stepping offsets in the spreading axis without significant overlap of topographic highs and two significant topographic saddles accompanied by a local narrowing of the topographic high without identifiable offset of the spreading axis (Table 2). All of the third-order RADs are the smallest offsets in the ridge axis we can resolve solely on the basis of multibeam bathymetry, but they correlate with variations in the volcanic structures observed independently by our near-bottom survey.

3. Volcanic Structures and Eruptive Style

3.1. Data Collection

Although the SeaBeam2000 system provides a very useful view of the regional bathymetry and ridge structure over kilometers of seafloor, the ability to resolve volcanic features that directly show eruptive style or the positions of volcanic vents is beyond the capability of any currently available near-surface swath mapping system. To achieve the high level of resolution needed to image fissures, volcanic vents, and lava flow fields, we used the near-bottom DSL-120 sonar system and the

Argo II photoacoustic sled during Leg 2 of the Sojourn expedition on R/V *Melville* in 1996 [*Haymon et al.*, 1997]. The DSL-120 side-scan sonar operates at 120 kHz and provides backscatter reflectivity imagery as well as phase bathymetry. We were able to image a 900-1000 m wide side-scan reflectivity swath, and a 700-800 m wide bathymetric swath, continuously along 150 km of ridge crest (Figure 1). Only one line was run using the DSL-120 sonar because the swath width was sufficient to cover the entire axial neovolcanic zone.

The DSL-120 survey provided a map for more detailed investigations using *Argo II*, a remotely operated vehicle providing data from three video cameras, two still cameras, Imagenex 675 kHz profiling sonar, 200 kHz side-scan sonar, conductivity-temperature-depth, transmissometer, and magnetometer [*Haymon et al.*, 1997]. The *Argo II* has a ~10 m visual swath width, and it is operated around-the-clock with real-time feedback. We obtained dense visual coverage of the axial neovolcanic zone on multiple tracks from 17°15'-17°40'S and 18°23'-18°29'S and coverage along a single track connecting these areas [*Haymon et al*., 1997]. These data allowed us to make lava morphology maps over large areas of the seafloor.

The *Argo II* visual observations of lava morphology were logged in real time into a geographic information system (GIS) database, but the observations were made at random intervals, and usually after crossing into an area where a new lava morphology was seen [*Haymon et al.*, 1997]. To estimate the area covered by a given lava morphology from the points logged along *Argo II* tracks, we followed the GIS method for buffering a line of navigation data into an effective swath width described by *Wright et al*. [1995]. Our procedure improves on this method by using average *Argo II* altitude for each line to calculate the average swath width along that line from field of view of the cameras. We converted each logged observation of lava morphology to an area within the visual swath width of *Argo II* by the "Thiessen" Polygon method (implemented by Environmental Systems Research Institute Arc/INFO® version 7.1). The principle of this method is that the entire area within the polygon surrounding each point (each logged observation in our case) is closer to that point than any other point defining any other polygon. This method was chosen because it preserves all of the original observations of lava morphology while providing a way to convert the nominal point data into nominal area data without creating overlapping areas. Problems with this point-to-area conversion method arise in determining precise locations of lava morphology contacts, particularly in places where observations were logged infrequently. While such problems make this method unsuitable for creating meter-scale geologic maps, the mix of lava morphologies are accurately represented when kilometers of ridge crest are statistically averaged. Where

detailed geological maps of lava morphology are required over smaller areas, as in the case of some of the lava domes described later, the aforementioned statistical methods were abandoned in favor of reviewing videotapes to precisely locate lava morphology contacts.

3.2. Lava Lakes With Overflow Tubes and Channels

Two areas of extensive collapse in the volcanic carapace at the crest of the smoothly domed part of the axial high were imaged at the meter-scale using the DSL-120 side-scan sonar system, and one was subsequently densely surveyed with the *Argo II* photoacoustic sled. These collapses are similar to the axial summit collapse trough at 9°26'-9°56'N on the EPR [*Haymon et al.*, 1991; *Fornari et al.*, 1998]. The northernmost collapse was discovered by the Cyana expedition in 1984 [*Renard et al.*, 1985] and named Aldo Lake by the Naudur Expedition in 1992 [*Auzende et al.*, 1996]. We refer to Aldo Lake and the entire string of collapses, 17°26'- 17°29'S, as the "Aldo Lake trough" (Figure 3). The southern string of collapses from 17°42' to 17°45'S was discovered during our 1996 DSL-120 sonar survey [*Haymon et al.*, 1997] and has been named "Pisco trough" (Figure 4).

Both of these areas of extensive collapses have a similar structure. The individual collapses are ~10-15 m deep (Figure 5). They are elongate parallel to the spreading axis and never more than 100 m wide. Both areas of extensive collapses continue for ~7 km along axis but consist of many individual elongate collapse pits that have an en echelon arrangement in many places. Visual investigation of these sites with *Argo II* showed very broad, flat lobate flows at the edges of the collapses. Most of the lobate crust surrounding the collapses covers cavernous voids that can be seen by looking back under the roof at the edge of the collapse. Lava pillars or continuous walls of coalesced pillars support the overhanging roof. Glassy selvages could be seen on the pillars and walls, and the floor of the collapses was mainly rubble or sheet flow. These observations suggest that these collapses are drained lava lakes [*Ballard et al.*, 1979; *Fornari et al.*, 1998].

Caved-in lava tubes and lava channels containing sheet flows were observed at the margins of the collapse troughs (Figure 3 and 4). None of the tubes or channels extend beyond the DSL-120 swath width. Lava flowing through the longest of these conduits would travel a total distance of <1 km, and the average flowline length is only 200 m. All of the identified conduit systems actually end <500 m in perpendicular distance from the collapse. The DSL-120 bathymetry shows that these large lava conduits are all no more than 6-8 m deep (Figure 5). Their distal ends terminate in lava deltas ~6-

8 m high (Figure 5) that look like inflated tube-fed pahoehoe flows on subaerial volcanoes [*Hon et al.*, 1994].

The same style of eruptions that created Aldo Lake and Pisco troughs may occur south of 17°56'S, although the overall structural style of the ridge is different. No such collapse troughs or associated lava distribution systems were observed south of 17°56'S, where the spreading axis runs through a graben bisecting the axial high. However, evidence of lava ponding and subsequent collapse is documented visually in the *Argo II* survey as well as by the Naudur Expedition dives [*Auzende et al.*, 1996] in the areas near 18°16' and 18°25'S. In these areas, large vertical scarps of the axial summit graben may dam the lava flows and cast acoustic shadows that make collapse troughs difficult to detect in DSL-120 side-scan records. When these two areas south of 17°56'S are included, the centers of four out of eight of the third-order segments are characterized by extensive volcanic collapse associated with drained lava lakes.

We observe that volcanic collapses, elongate parallel to the spreading axis, are the source of lava tubes and sheet flows and are the loci of hydrothermal flow [*Haymon, et al.*, 1997; *O'Neill*, 1998]. We hypothesize that these collapse features form directly over eruptive fissures, like troughs of similar dimensions found on other ridges [*Fornari et al.*, 1998; *U.S. Geological Survey Juan de Fuca Study Group*, 1986]. Fissure eruptions in Iceland and Hawaii [e.g., *Sigurdsson and Sparks*, 1978; *Holcomb*, 1987; *Lockwood et al.*, 1987] produce en echelon segments similar in length and offset to the SEPR collapsed lava lakes. The *Argo II* video reveals that the margins of the collapses have sheet flow lava morphology that appears to be generated from a line source eruption similar to historical fissure eruptions of basaltic volcanoes. The local lava morphology of primarily smooth lobates and sheet flows and the occurrence of a relatively thin roof over large areas of void space adjacent to the collapses suggest a rapid, high effusion rate eruption [*Bonatti and Harrison*, 1988; *Griffiths and Fink*, 1992; *Gregg and Fink*, 1995; *Gregg et al.*, 1996]. Hydrothermal venting issuing directly from fissures and breccia piles on the floor of the collapse is a key observation to support the interpretation that collapses form directly over the eruptive fissures [*O'Neill*, 1998]. Eruptive fissures can provide both a pathway for fluid flow and a heat source that is large enough to power hydrothermal circulation [*Haymon et al.*, 1993; *Wright et al.*, 1995; *U.S. Geological Survey Juan de Fuca Study Group*, 1986].

3.3. Axial Basaltic Lava Domes

Small domed volcanic edifices form on the ridge axis mainly in areas away from the collapsed lava lake complexes and unassociated with lava channels. These axial volcanic edifices are subtle topographic features which average 200 m in diameter and 20 m in height. These axial edifices were identified in both the DSL-120 side-scan backscatter imagery and bathymetry as local topographic highs with a quasi-elliptical base. Some coalesce into rows aligned with the ridge axis, as if erupting from an axis-parallel fissure, but the outlines of discrete structures can still be traced (Figure 6). Axial edifices are also found as isolated features or in small clusters. We classify the small domed edifices on the SEPR ridge crest as "lava domes" because our observations fit that genetic classification, although they are similar to constructs generically called "pillow mounds" [e.g., *Perfit and Chadwick*, 1998]. We describe below in detail how the SEPR axial lava domes fit the definition of lava domes as volcanic edifices built by lava piling up over a primary volcanic vent [*Williams*, 1932]. The differentiation of pillow lava domes from other types of pillow mounds is warranted at this stage since some studies imply that pillow mounds found in certain settings may be secondary, tube-fed or lava flow inflation features which would have much different implications for volcanic systems and eruption mechanics [*Appelgate and Embley*, 1992; *Bryan et al*., 1994; *Smith and Cann*, 1999].

Are the dome-shaped features imaged by the DSL-120 sonar true lava domes? Lava domes form directly over primary volcanic vents fed directly by dikes, not from rootless vents fed by surface lava flows. Distinguishing volcanic vents from rootless vents provides insight about how the axial magma delivery system creates topography at the ridge axis. The presence of a lava dome implies that an underlying primary vent erupted relatively short, slow moving lava flows. In contrast, rootless volcanic constructions, such as tumuli and hornitos, form in relatively long lava flows with well-organized lava tube systems that require steady eruptions lasting several days or longer to develop [e.g., *Calvari and Pinkerton*, 1998; *Keszthelyi and Self*, 1998; *Hon et al.*, 1994; *Walker*, 1991].

The visual observations made with *Argo II* help to establish that the axial lava domes imaged by the DSL-120 sonar form over primary volcanic vents. Review of the video from *Argo II* reveals that the domes are made mainly of pillow lava, with minor lobate lava flows primarily found near the summits of some of the larger domes (Figure 7). Tumuli form exclusively in inflated lava fields, but since pillow lava is not generally associated with extensive lava fields on the SEPR and since the axial lava domes do not appear to be part of any extensive flow field [*Haymon et al.*, 1997], we infer that the

axial lava domes formed over primary volcanic vents. Further evidence that axial volcanic mounds are not rootless cones is that hydrothermal sulfide chimneys commonly grow near fissures or collapses on the mounds [*O'Neill*, 1998] (Figure 7). This level of hydrothermal activity requires a significant sustained heat source, such as an intrusion creating an eruption at a volcanic vent. A single lava flow, even long-duration inflation of a flow field, would not be able to provide enough heat to power several hydrothermal chimneys. All of this evidence suggests that axial lava domes described here form by eruptions from primary volcanic vents.

Although the preceding evidence suggests that the axial lava domes are not secondary volcanic constructions fed from surface lava flows, seafloor mapping alone cannot detect subsurface conduits, such as preexisting lava tubes. Lava supplied along strike from the segment center through reoccupied lava tubes would appear to have many of the qualities of primary volcanic vents. However, a simple calculation of the pressure gradient in a lava tube along the crest of the gently sloping SEPR suggests that gravity-driven flow through lava tubes is unlikely to create axial lava domes near segment ends. Assuming gravity-driven Poiseulle flow of lava in a cylindrical tube, the elevation drop E_d required to produce a flow at the end of the tube is given by $E_d = 8\mu QD/\pi R^4(p_l - p_w)g$ [*Turcotte and Schubert*, 1982]. Reasonable values for this equation are a lava viscosity $\mu=10^2$ Pa s [*Head et al.*, 1996]; lava density p_l=2500 kg/m^3 [*Head et al.*, 1996]; water density p_w=1000 kg/m^3 ; typical volume flux through the tube Q=5 m^3/s (as reported for subaerial flows by *Kauahikaua et al.* [1998]); a lava tube radius R=3 m (matching the size of the largest collapsed lava tube seen in DSL120 records on the SEPR), and gravitational acceleration on Earth g=9.8 m/s^2. The minimum elevation drop theoretically required to form a pillow flow without any height at a distance D of 1 km from the segment center is roughly 10 m. Along the SEPR, topographic gradients are generally much less than 10 m/km, thus making it improbable that axial volcanic mounds are built 20 m high over secondary vents. On the Mid-Atlantic Ridge the steeper topographic gradients might allow volcanic structures like the lava domes seen on the SEPR to form over secondary vents [*Smith and Cann*, 1999].

Axial pillow domes are distinguishable from lava shields, though both are primary volcanic edifices formed by small, nonexplosive eruptions. Lava shields are built from lava flows that reach far from their vent, resulting in a very low slope profile and an extensive apron of lava flows surrounding the shield [*Walker*, 2000; *Rossi*, 1996]. In contrast, the SEPR axial pillow domes appear to cover fairly small areas and are not the source of extensive lava flows. The ratio of edifice height to basal radius

can be used to discriminate between a lava dome composed of short flows that construct a high edifice with a small basal radius and a lava shield composed of long flows that construct a low edifice with larger basal radius. The height:radius ratio of the SEPR axial lava domes is closer to that of other basaltic lava domes than that of basaltic lava shields (Figure 8). This suggests that SEPR axial lava domes, although composed of basalt, generally have much shorter lava flows and possibly more endogenic growth than the low-relief lava shields on land.

Dome-forming basaltic eruptions are uncommon on land where the growth of lava flow crust is too slow to impede the expansion of the flow near the vent. Quenching of lava in the submarine environment could create a thick crust quickly enough and with sufficient strength to inhibit the spreading of lava when the effusion rate is low. This would favor the formation of basaltic lava domes during low effusion rate submarine eruptions. Basaltic lava domes in a forearc extensional setting were studied after being exposed on an island and were interpreted to have formed by endogenous growth in a submarine environment [*Smellie et al.*, 1998].

3.4. Axial Lava Domes Mark the Ends of Third-Order Segments

A clear correlation that emerged from the Sojourn 2 survey data was the large number of axial domes near the ends of segments. To quantify this systematically, we digitized the outline of the base of each dome and calculated its position as a point at the centroid of its base. The distance from the centroid of the dome to the nearest segment boundary was determined by straight line distance between the centroid point and the segment endpoint. Separate calculations were made for the OSC-bounded segments, for all of the third-order segments identified in multibeam bathymetry maps, and for the fourth-order segments identified in the DSL-120 sonar data. Because the segments have different lengths, we used a normalized distance along the segment. The distance from dome to segment end was divided by half of the total length of the segment to get the normalized distance. This normalization method was employed for the total edifice distribution, the total base coverage, and the average basal area of the axial domes. The results were graphed using bins representing 20% of the distance from the segment end to segment center.

When normalized to the OSC-bounded segments only, the distribution of axial lava domes shows a bimodal distribution (Figure 9a). The abundance of domes increases at both the centers and the ends of segments. The explanation for this is that other RADs exist near the centers of some of the OSC-bounded segments. When all third-order segments in the survey area are used (Table 2), the

abundance of axial lava domes decreases from segment end to segment center (Figure 9b). Dome size, represented by average basal area of the mounds in each bin, shows the opposite relationship, decreasing near third-order RADs (Figure 10).

A finer scale of discontinuity (fourth-order) was identified within the DSL-120 records, where offsets of <200 m can be detected [*Haymon et al*, 1997]. When the distribution of either the number of domes or their average basal area is normalized to these very short segments, no patterns emerge (Figure 9c). Thus the formation of axial lava domes does not appear to be controlled by processes operating at the smallest scale of segmentation.

3.5. Lava Morphology

By comparing submarine lava flow morphology and volcanic structures to features created by subaerial volcanism, inferences can be made about eruption dynamics on mid-ocean ridges [e.g., *Ballard et al.*,1979]. Low effusion rate, slowly advancing pahoehoe flows become pillow flows when they enter the water [*Jones*, 1968; *Moore*, 1975]. The flat, often lineated or autobrecciated, surfaces of submarine sheet lava flows are usually interpreted as indicators of high lava effusion rate [e.g., *Ballard et al.*,1979; *Gregg and Fink*, 1995]. Sheet flows are observed mainly in just two environments in our *Argo II* survey: (1) floors and margins of collapsed lava lakes, and (2) floors and levees of lava channels (Figures 3 and 4). These observations are consistent with the idea that submarine sheet flows form by rapidly flowing (high effusion rate) lava, analogous to subaerial lava ponds and channels [*Wolfe*, 1988; *Peterson et al.*, 1994]. The inferences from subaerial analogues are supported by laboratory studies showing that low effusion rate eruptions produce pillow lava flows and that effusion rates an order of magnitude higher can produce sheet lava flows [*Griffiths and Fink*, 1992; *Gregg and Fink*, 1995].

Because the distribution of lava domes and collapse troughs along the ridge suggests that effusion rate varies systematically over the third-order segments, we quantified the along-axis distribution of lava morphology as an independent indicator of changes in volcanic effusion rate. The highly variable nature of lava morphology requires almost complete visual coverage for accurate mapping, and statistical methods are the most efficient way of dealing with the large quantity of raw data this generates. Dense coverage of the ridge crest that we obtained with *Argo II* from 17°15’ to 17°40’S provides an ideal data set which encompasses the three northernmost third-order segments of our study area [*Haymon et al.*, 1997].

The real-time observations from *Argo II* of lava morphology were assigned to one of three lava morphology categories: (1) pillow, (2) lobate, and (3) sheet. The discontinuous observations were expanded into areas, where each area is more proximal to the observation "point" location than any other observation, and is clipped by the actual *Argo II* camera field of view. The lava morphology was binned at 20% of the distance from segment end to segment center, following the method described for the axial lava domes. The total area covered by each of the three lava morphologies was divided by the total area of *Argo II* coverage to normalize the data set to 100% of the coverage area within each bin.

When the data from the three northernmost segments of our survey are stacked and binned at 20% of the segment length, the lava morphology exhibits a regional pattern consistent with the observed distribution of volcanic structures on the ridge axis (Figure 11). At segment ends the most common lava morphology is pillow lava, and the volcanic structures are axial lava domes. Both indicate that low effusion rate eruptions are most common near the ends of third-order segments. At segment centers, lobate lava flows cover most of the area, and the characteristic volcanic structures are large collapses. Furthermore, sheet lava flows are insignificant at segment ends but common at the segment center. Surrounding Aldo Lake trough, sheet flows are extensive (> 50% of the total area surveyed). We conclude that lava effusion rates are consistently higher near the centers of third-order segments. The regional changes in lava morphology seen in the *Argo II* survey support our interpretation that the volcanic structures seen with DSL-120 reveal changes in the effusion rate of eruptions over third-order segments (Figure 11).

4. Discussion of Volcanic Segmentation

Systematic changes in volcanic morphology along third-order segments show that the eruption dynamics vary at this length scale (Figure 11). Because changes in the eruption dynamics reflect changes in the delivery of magma to volcanic vents, the magma plumbing system also varies at this scale. Hence we propose that along-axis changes in eruptive style corresponding to third-order segmentation reveal that each third-order segment physically behaves as a single volcanic system (as in the Icelandic usage [e.g., *Gudmundsson*, 1995]) with higher effusion rates above centrally located vents and lower effusion rates at vents near segment ends. While third-order RADs on slow-spreading ridges are gaps between large volcanic edifices on the floor of the median valley

[*Macdonald et al.*, 1991; *Smith et al.*, 1999], their analogues at fast spreading rates are topographically subtle features such as small offsets (<1 km) or saddle points in axial topography.

4.1. Axial Lava Dome Formation

A lower bound on longevity of eruptive activity at individual axial domes may be approximated by measuring the volume of the dome and dividing it by a theoretical volumetric flow rate appropriate for the lava morphology on the mound. This calculation assumes the entire edifice is created by continuous activity from a point source vent. The population of axial domes has an average volume of $4x10^5$ m^3 and a maximum individual volume of $8x10^6$ m^3. Mapping the lava morphologies with *Argo II* reveals that the axial lava domes are primarily covered by pillow basalt (Figure 7). Various estimates can be obtained for the volumetric flow rate of pillow basalt based on models and observations in different environments. Laboratory simulations indicate that an effusion rate from 1-100 m^3/sec could form pillow basalt [*Gregg and Fink*, 1995]. Observations of flowing pillow basalt on the coast of the island of Hawai'i suggest that an average rate of 1 m^3/s may be an appropriate approximation [*Moore*, 1975; *Tribble*, 1991]. At an average-sized dome where $4x10^5$ m^3 of basalt erupts at a rate of 1 m^3/sec., the whole edifice can be built in ~4 days. Even for the largest axial lava dome found, a calculation for the effusion rate of 1 m^3/s shows that it would take only 4 months of continuous eruption to form. These results indicate durations that are similar to the 6 day eruption of an ~1 km long fissure in the spreading center in Afar [*Allard et al.*, 1979].

Chains of axial lava domes that have been mapped here (Figures 6 and 7) and on the southern Juan de Fuca Ridge [*Chadwick and Embley*, 1994] may form much like the development of a "crater row" along a subaerial eruptive fissure [e.g., *Thorarinsson*, 1969; *Thorarinsson and Sigvaldason*, 1972; *Bjornsson et al.*, 1977; *Sigurdsson and Sparks*, 1978; *Lockwood et al.*, 1987]. In subaerial fissure eruptions, linear "curtain of fire" geysering becomes focused to a small number of volcanic centers within a few hours to days depending on the effusion rate and viscosity of the lava [*Wylie et al.*, 1999]. Crater rows along fissure swarms in Iceland often form by lateral dike injection along tectonic rift zones [*Sigurdsson and Sparks*, 1978]. During the 1978 Krafla eruption, the rate of flow in the dike was calculated as decreasing with increasing distance from Krafla caldera [*Sigurdsson*, 1987]. This is a consequence of a more constricted magma conduit that reduces the magma flow toward the propagating dike tip [*Hardee*, 1987; *Rubin and Pollard*, 1987]. By analogy, we suggest that the reduction of overall mass flux at the propagating end of a dike creates the along-axis change that we

observe along third-order segments from sheet-lobate lava lakes near segment centers to pillow lava domes near segment ends.

The 1998 eruption of Axial Volcano on the Juan de Fuca Ridge afforded an unprecedented opportunity to observe the pattern of submarine volcanism along the length of a laterally intruded dike. A lateral dike propagation event down the South Rift of Axial Volcano from its caldera was tracked seismically for 10 days in 1998 [*Dziak and Fox*, 1998]. The eruption associated with this dike intrusion was mapped as a sheet flow in Axial caldera, at the proximal end of the dike, and pillow flow at the far end of the eruption [*Embley et al.*, 1999]. The eruption of the Cleft segment of the Juan de Fuca ridge in the 1980s also produced sheet flows associated with collapsed lava lakes near the segment center and "pillow mounds" at the segment end without the anomalous magma supply associated with Axial Volcano [*Embley and Chadwick*, 1994]. The progression of lava flow morphology documented along intruding dikes on northeast Pacific spreading centers is the same pattern that we observe along third-order segments on the SEPR. If lateral dike propagation is the cause of the observed pattern in volcanic morphology, it requires focusing the magma supply beneath the central parts of ridge segments to give the dikes a center from which to propagate.

4.2. Evidence for Segmentation of the Magma Supply

Along-axis geochemical variations in both the major and trace element ratios highlights differences in the parental composition of the magma supply, thus defining a magmatic segmentation of the EPR on the basis of lavas derived from different parental magmas [*Langmuir et al.*, 1986; *Sinton et al.*, 1991; *Reynolds et al.*, 1992]. These magmatic segments correspond almost perfectly with the structural segmentation of the ridge axis, but sample spacing (average ~10 km) is too wide to discern all of the fine-scale magmatic segments [*Batiza and Margolis*, 1986; *Langmuir et al.*, 1986; *Sinton et al.*, 1991]. In our study area, four magmatic segment boundaries were identified by differences among a suite of major and trace elements in glass analyses from dredged rocks [*Sinton et al.*, 1991]. The magmatic segments correspond to third-order RADs (Figure 1b). However, the dredge samples were too widely spaced to be able to define all of the morphologic third-order segments that we observe. Work now in progress on rock samples collected at a closer spacing by wax cores and submersible dives hints that additional magmatic segments may exist on the SEPR [*Bergmanis et al.* 1999; *Sinton et al.*, 1999].

Sinton et al. [1991] pointed out that the distinctive parental magma composition defining each magmatic segment on the SEPR requires a discrete magma injection system for each segment. Seismic tomography indicates that the magma supply to second-order ridge segments has a three-dimensional organization beginning far below the crust [*Dunn and Toomey*, 1997; *MELT Seismic Team*, 1998]. Closer to the seafloor, the magma supply may focus into finer-scale magmatic injection centers.

The breaks in continuity and local depth maxima of the AMC closely match the location of third-order RADs, and abundance of axial pillow lava domes within the study area (Figure 12). The only breaks in the AMC reflector occur beneath the two largest third-order OSCs in the study area where pillow lava domes are also found in abundance. Yet, even where there is no break in the AMC reflector, all local depth maxima of the AMC reflector are located within the zones of third-order RADs (Figure 12). The most significant local increases in the AMC reflector depth coincide with those RAD zones with the greatest numbers of axial pillow domes, whereas smaller increases in AMC depth seem to be associated with fewer pillow domes at the seafloor. These local maxima may indicate places where the magma chamber is segmented. For example, seismic imaging within a second-order segment at 14°-16°S on the EPR (north of our survey area) suggests that the apparently continuous AMC actually contains several pockets of pure melt separated by crystalline mush zones [*Singh et al.*, 1998].

Sonar and geological mapping, along- and across-axis seismic profiles, and submersible-collected rock samples from Aldo Lake trough at 17°27’S to the pillow mounds in the zone of offset near 17∞30’S permit a rare opportunity to integrate all of these data sets to examine the nature of a volcanic segment in detail (Figure 13). Seismic lines across axis show a deepening (from 1000 to 1210 m) and narrowing (from 1540 to 740 m) of the AMC from Aldo Lake to the RAD [*Hooft et al.*, 1997]. The width over which layer 2A thickens also reduces significantly (from 7.1 to 3.4 km) [*Carbotte et al.*, 1997]. Rock samples collected on one side of the RAD at 17°30’S have different liquid lines of descent from those collected just on the other side, suggesting a break in the volcanic plumbing system [*Bergmanis et al.*, 1999]. The combined evidence of a segmented magma supply from seismic and geochemical measurements is consistent with our hypothesis, based on the pattern of volcanic morphology, that the SEPR is organized into volcanic systems at the third-order segment scale.

4.3. Significance of Volcanic Segmentation at Fast Spreading Ridges

We propose that a "volcanic segment" of a fast spreading mid-ocean ridge is essentially synonymous with a "volcano" in other settings where eruptions tend to form volcanic edifices. The broad definition of a volcano is a system of volcanic vents tapping a common magma supply to build a volcanic structure [*Simkin and Siebert*, 2000]. However, the thin lithosphere at the SEPR has a low flexural rigidity that prevents building a large volcanic edifice on the axis [*Buck et al.*, 1997]. Rather than being a constructional volcanic ridge, the axial high of a fast spreading ridge is thought to be an isostatic or flexural feature [*Madsen et al.*, 1984; *Eberle and Forsyth*, 1998]. Because the axial highs of the SEPR and other fast-spreading ridges are isostatic rises instead of being constructional ridges, the highest points on the ridge do not mark the centers of individual volcanic constructions. For this reason, seismic layer 2A is consistently thinnest along the axis of the ridge, but if the rise were a volcanic construction, it would be thickest at the axis [*Carbotte and Macdonald*, 1994; *Hooft et al.*, 1996]. Thus the elevated topography of the ridge axis on fast spreading ridges cannot be directly compared to constructional volcanic ridges like those found in the median valley of slow spreading ridges [*Smith et al.*, 1999]. The significance of third-order segmentation is that it reveals the discrete volcanic systems comprising the ridge in the absence of large volcanic constructions.

In this context, what are fourth-order segments? The RADs defining fourth-order segment boundaries are so fine that near-bottom high-resolution images or very dense suites of rock samples are usually required to notice them. As originally defined [*Langmuir et al.*, 1986; *Macdonald et al.*, 1988], they are probably segments of eruptive axial fissures. While third-order segments may remain distinct for hundreds to thousands of years, they cannot persist for longer than 10^3-10^5 years, or else they would create an off-axis discordant zone. Even more ephemeral, fourth-order segments may persist as distinct segments for just tens to hundreds of years, changing with each new crack propagation and eruptive episode (Table 1). This order of segmentation may be significant on the timescales and length scales that most directly affect along-axis variations in hydrothermal activity [*Haymon et al.*, 1991, 1993].

If third-order segments represent individual volcanic segments on mid-ocean ridges, why did the 1989 *Argo* survey on the East Pacific Rise, 9°09'-9°54'N, ridge crest fail to reveal the patterns of volcanism observed on the SEPR [*Haymon et al.*, 1991]? Sonar coverage comparable to our DSL-120 survey was not available for the northern EPR at the time of the *Argo* survey. A recently completed

DSL-120 sonar survey indicates that the pattern of volcanic segmentation described here applies to the EPR at 9°-10°N (D. Fornari, M. Perfit, M. Tolstoy, R. Haymon, D. Scheirer, P. Johnson, G. Kurras, S. White, J. Getsiv, and shipboard scientific party, Shipboard data web site compiled during R/V *Melville* NEMO Expedition, Leg 2, http://128.128.21.37/, 2000). Basaltic lava domes are more abundant at the end of third-order segment, while indicators of high effusion rates are more prevalent at the center of third-order segments at 9°-10°N [*White et al*., 2000].

5. Speculations

Two observations invite further comment. First, along-strike changes in the width of the zone over which seismic layer 2A thickens may correlate with volcanic segmentation (wider near midsegment). Second, the pattern of axial lava dome distribution on third-order segments is similar to the pattern of isolated, off-axis volcano distribution on second-order segments (more but generally smaller at segment ends [*White et al.,* 1998]).

The best studied third-order segment in our survey area is the segment from 17°18.5' to 17°30'S. This segment contains the Aldo Lake trough, which is located just to the south of the geographic center of the segment (Figure 13). Seismic reflection profiles across this third-order segment show that seismic layer 2A increases in thickness from ~140 m at the center to ~170 m at the ends of the segment, although these changes are within the uncertainty of the measurements [*Carbotte et al.,* 1997]. Off axis, layer 2A increases in thickess to ~500 m; however, it reaches this values anywhere from <1 km to >3 km from the ridge axis [*Carbotte et al.,* 1997; *Hooft et al.,* 1997]. The average total width over which layer 2A thickens rapidly is ~7 km at midsegment, but is only ~5 km at the segment ends [Carbotte et al., 1997] (Figure 13). The interpretation of layer 2A as volcanic pile is favored by seismologists currently [*Hooft et al.,* 1996; *Carbotte et al.,* 1997], but alternative explanations for the low seismic velocities are a metamorphic alteration or a crustal cracking front [*Spudich and Orcutt,* 1980; *McClain et al.,* 1985; *Rohr et al.,* 1988]. If layer 2A is the volcanic pile, our geological mapping along this segment suggests an explanation; lava flows extend farther from the ridge axis near the segment center, where Aldo Lake is located. The lava conduits around the Aldo Lake trough appear to transport lava as far as ~1 km away from the axis (Figure 3). At the segment ends, axial lava domes contribute to thickening the volcanic layer no farther than a few hundred meters from the axis. If this same pattern of eruptions is sustained, then our observations are consistent with a wider zone of seismic layer 2A thickening caused by the accumulation of lava flows over a wider

neovolcanic zone near from the centers of volcanic segments. If layer 2A is not the volcanic layer, then we cannot explain the correlation we observe. The hypothesized alternatives would require that fissure development or a metamorphic alteration front extends farther from the ridge axis near midsegment than at segment ends.

Some near-ridge volcanoes could have originated as axial lava domes that continued to grow as spreading rafted them farther from the ridge axis. Pillow lava constructions have been investigated and sampled on the sides of the axial high on the northern EPR [*Perfit et al*., 1994]. The distribution of axial lava domes relative to third-order segmentation (more but smaller lava domes near segment ends) is similar to the distribution of isolated off-axis volcanoes relative to second-order segmentation (more but smaller volcanoes near segment ends) [*White et al*., 1998]. The similarity of these two patterns is consistent with a hypothesized hierarchy of segmentation of the ridge axis magma supply [*Batiza*, 1996; *Macdonald*, 1998] and suggests that more fundamental levels of magmatic segmentation affect volcanic processes farther from the ridge axis. Further investigations will be necessary to find to what extent off-axis volcanism may have evolved from the volcanic segmentation of the ridge axis.

6. Conclusion

The volcanic morphology and structures formed on the SEPR vary systematically over third-order segments such that inferred effusion rates are lower and lava flows are shorter at segment ends. Volcanic edifices in the form of small basaltic lava domes are found on the axis of fast-spreading ridges in increasing abundance toward third-order RADs. In contrast to the collapsed lava lakes that occur near the centers of some of the third-order segments, the lava domes reflect a decrease in overall effusion rate toward segment ends. The collapsed lava lakes are associated with thin-crusted, hollow lobate lava flows and sheet lava flows, and collapses in the lobates suggest that these flows have inflated several meters in areas proximal to the eruptive vent. The general pattern of decreasing effusion rate away from the centers of third-order segments suggests the volcanic processes at superfast spreading ridges are fundamentally segmented at this scale.

References

Allard, P., H. Tazieff, and D. Dajlevic, Observations of seafloor spreading in Afar during the November 1978 fissure eruption, *Nature, 279*, 30-33, 1979.

Appelgate, B., and R. W. Embley, Submarine tumuli and inflated tube-fed lava flows on Axial Volcano, Juan de Fuca Ridge, *Bull. Volcanol., 54*, 447-458, 1992.

Auzende, J.-M., et al., Recent tectonic, magmatic, and hydrothermal activity on the East Pacific Rise between 17°S and 19°S: Submersible observations, *J. Geophys. Res., 101*, 17,995-18,010, 1996.

Ballard, R. D., R. T. Holcomb, and T. H. van Andel, The Galapagos Rift at 86°W, 3., Sheet flows, collapse pits and lava lakes of the rift, *J. Geophys. Res., 84*, 5407-5422, 1979.

Barth, G. A., and J. C. Mutter, Variability in oceanic crustal thickness and structure: Multichannel seismic reflection results from the northern East Pacific Rise, *J. Geophys. Res., 101*, 17,951-17,976, 1996.

Batiza, R., Magmatic segmentation of mid-ocean ridges: A review, in *Tectonic, Magmatic, Hydrothermal, and Biological Segmentation of Mid-Ocean Ridges*, edited by C. J. Macleod, P. A. Tyler, and C. L. Walker, *Geol. Soc. Am. Spec. Pub., 1*, 103-130, 1996.

Batiza, R., and S. Margolis, Small non-overlapping offsets of the East Pacific Rise, *Nature, 320*, 439-441, 1986.

Bergmanis, E. C., J. M. Sinton, S. White, K. Macdonald, R. Batiza, K. Rubin, T. K. P. Gregg, C. L. Van Dover, and K. Grÿnvold, Anatomy of a mid-ocean ridge volcanic eruption: The Aldo-Kihi flow between 17°24'S and 17°34'S, East Pacific Rise, *Eos Trans. AGU., 80*(46), Fall Meet. Suppl., F1075, 1999.

Bjornsson, A., K. Saemundsson, P. Einarsson, E. Tryggvason, and K. Gronvold, Current rifting episode in north Iceland, *Nature, 266*, 318-323, 1977.

Bonatti, E., and C. G. A. Harrison, Eruption style of basalt in oceanic spreading ridges and seamounts: Effect of magma temperature and viscosity, *J. Geophys. Res., 93*, 2967-2980, 1988.

Bryan, W. B., S. E. Humphris, G. Thompson, and J. F. Casey, Comparative volcanology of small axial eruptive centers in the MARK area, *J. Geophys. Res., 99*, 2973-2984, 1994.

Buck, W. R., S. M. Carbotte, and C. Mutter, Controls on extrusion at mid-ocean ridges, *Geology, 25*, 935-938, 1997.

Calvari, S. and H. Pinkerton, Formation of lava tubes and extensive flow field during 1991-1993 eruption of Mount Etna, *J. Geophys. Res., 103*, 27,291-27,301, 1998.

Canales, J. P., R. S. Detrick, S. Bazin, A. J. Harding, and J. A. Orcutt, Off-axis crustal thickness across and along the East Pacific Rise within the MELT area, *Science, 280*, 1218-1220, 1998.

Carbotte, S., and K. C. Macdonald, The axial high at intermediate and fast spreading ridges, *Earth Planet. Sci. Lett., 128*, 85-97, 1994.

Carbotte, S., J. C. Mutter, and L. Xu, Contribution of tectonism and volcanism to axial and flank morphology of the southern EPR from a study of layer 2A geometry, *J. Geophys. Res., 102,* 10,165-10,185, 1997.

Chadwick W. W., and R. W. Embley, Lava flows from a mid-1980s submarine eruption on the Cleft Segment, Juan de Fuca Ridge, *J. Geophys. Res., 99,* 4761-4776, 1994.

Cochran, J. R., J. A. Goff, A. Malinverno, D. J. Fornari, C. Keeley, and X. Wang, Morphology of a "superfast" mid-ocean ridge crest and flanks: The East Pacific Rise, 7°-9° S, *Mar. Geophys. Res., 15,* 65-75, 1993.

Cormier, M.-H., and K. C. Macdonald, East Pacific Rise 18°S-19°S: Asymmetric spreading and ridge reorientation by ultra-fast migration of ridge axis discontinuities, *J. Geophys. Res., 99,* 543-564, 1994.

Cormier, M.-H., D. S. Scheirer, K. C. Macdonald, R. M. Haymon, S. White, and Sojourn 1 Science Party, A geophysical survey of the East flank of the East Pacific Rise at 15°-20°S, *Eos Trans. AGU, 77*(46), Fall Meet. Suppl., F660, 1996.

DeMets, C., R. G. Gordon, D. F. Argus, and S. Stein, Current plate motions, *Geophys. J. Int., 101,* 425-478, 1990.

Detrick, R. S., A. J. Harding, G. M. Kent, J. A. Orcutt, J. C. Mutter, and P. Buhl, Seismic structure of the Southern East Pacific Rise, *Science, 259,* 499-503, 1993.

Devine, J. D., and H. Sigurdsson, Petrology and eruption styles of Kick'Em-Jenny submarine volcano, Lesser Antilles island arc, *J. Volcanol. Geotherm. Res., 69,* 35-58, 1995.

Dunn, R. A., and D. R. Toomey, Seismological evidence for three-dimensional melt migration beneath the East Pacific Rise, *Nature, 388,* 259-262, 1997.

Dziak, R. P., and C. G. Fox, Hydroacoustic detection of submarine volcanic activity at Axial Volcano, Juan de Fuca Ridge, January 1998, *Eos, Trans. AGU, 79*(45), Fall Meet. Suppl., F921, 1998.

Eberle, M. A., and D. W. Forsyth, An alternative dynamic model of the axial topographic high at fast spreading ridges *J. Geophys. Res., 103,* 12,309-12,320, 1998.

Embley, R. W., and W. W. Chadwick, Volcanic and hydrothermal processes associated with a recent phase of seafloor spreading at the northern Cleft segment: Juan de Fuca Ridge, *J. Geophys. Res., 99,* 4741-4760, 1994.

Embley, R. W., W. W. Chadwick, D. Clague, and D. Stakes, 1998 eruption of Axial Volcano: Multibeam anomalies and seafloor observations, *Geophys. Res. Lett., 26,* 3425-3428, 1999.

Fornari, D. J., R. M. Haymon, M. R. Perfit, T. K. P. Gregg, and M. H. Edwards, Axial Summit Trough of the East Pacific Rise 9°N to 10°N: Geological characteristics and evolution of the axial zone on fast-spreading mid-ocean ridges, *J. Geophys. Res., 103*, 9827-9855, 1998.

Gente, P., J. M. Auzende, V. Renare, Y. Fouquet, and D. Bideau, Detailed geological mapping by submersible of the East Pacific Rise axial graben near 13°N, *Earth Planet. Sci. Lett., 78*, 224-236, 1986.

Gregg, T. K. P., and J. H. Fink, Quantification of submarine lava-flow morphology through analog experiments, *Geology, 23*, 73-76, 1995.

Gregg, T. K. P., D. J. Fornari, M. R. Perfit, R. M. Haymon, and J. H. Fink, Rapid emplacement of a mid-ocean ridge lava flow on the East Pacific Rise at 9°46'-51'N, *Earth Planet. Sci. Lett., 144*, E1-E7, 1996.

Griffiths, R. W., and J. A. Fink, Solidification and morphology of submarine lavas; a dependence on extrusion rate, *J. Geophys. Res., 97*, 19,729-19,737, 1992.

Gudmundsson, A., Infrastructure and mechanics of volcanic systems in Iceland, *J. Volcanol. Geotherm. Res., 64*, 1-22, 1995.

Hardee, H. C., Heat and mass transport in the east-rift-zone magma conduit of Kilauea Volcano, in *Volcanism in Hawaii*, edited by R. W. Decker, T. L. Wright and P. H. Stauffer, *U.S. Geol. Surv. Prof. Pap., 1350*, 1471-1486, 1987.

Haymon, R. M., D. J. Fornari, M. H. Edwards, S. M. Carbotte, D. Wright, and K. C. Macdonald, Hydrothermal vent distribution along the East Pacific Rise crest (9°09'-54'N) and its relationship to magmatic and tectonic processes on fast-spreading mid-ocean ridges, *Earth Planet. Sci. Lett., 104*, 513-534, 1991.

Haymon, R. M., et al., Volcanic eruption of the mid-ocean ridge along the East Pacific Rise crest at 9°45-52'N: Direct submersible observations of seafloor phenomena associated with an eruption event in April, 1991, *Earth Planet. Sci. Lett., 118*, 85-101, 1993.

Haymon, R. M., et al., Distribution of fine-scale hydrothermal, volcanic, and tectonic features along the EPR crest, 17°15'-18°30'S: results of near-bottom acoustic and optical surveys, *Eos Trans. AGU, 78*(46), Fall Meet. Suppl., F705, 1997.

Head, J. W., L. Wilson, and D. K. Smith, Mid-ocean ridge eruptive vent morphology and structure: evidence for dike widths, eruption rates, and evolution of eruptions and axial volcanic ridges, *J. Geophys. Res., 101,* 28,265-28,280, 1996.

Holcomb, R. T., Eruptive history and long-term behavior of Kilauea Volcano, in *Volcanism in Hawaii*, edited by R. W. Decker, T. L. Wright and P. H. Stauffer, *U.S. Geol. Surv. Prof. Pap., 1350,* 261-350, 1987.

Hon, K., J. Kauahikaua, R. Denlinger, and K. Mackay, Emplacement and inflation of pahoehoe sheet flows: Observations and measurements of active lava flows on Kilauea Volcano, Hawaii, *Geol. Soc. Am. Bull., 106,* 351-370, 1994.

Hooft, E. E. E., H. Schouten, and R. S. Detrick, Constraining crustal emplacement processes from the variation in seismic layer 2A thickness at the East Pacific Rise, *Earth Planet. Sci. Lett., 142,* 289-309, 1996.

Hooft, E. E. E., R. S. Detrick, and G. M. Kent, Seismic structure and indicators of magma budget along the southern East Pacific Rise, *J. Geophys. Res., 102,* 27,319-27,340, 1997.

Jones, J. G., Pillow lava and pahoehoe, *J. Geol., 76,* 485-488, 1968.

Kauahikaua, J., K. V. Cashman, T. N. Mattox, C. C. Heliker, K. A. Hon, M. T. Mangan, and C. A. Thornber, Observations on basaltic lava streams in tubes from Kilauea Volcano, island of Hawai'i, *J. Geophys. Res., 103,* 27,303-27,324, 1998.

Keszthelyi, L., and S. Self, Some physical requirements for the emplacement of long basaltic lava flows, *J. Geophys. Res., 103,* 27,447-27,464, 1998.

Langmuir, C. H., J. F. Bender, and R. Batiza, Petrological and tectonic segmentation of the East Pacific Rise, 5°30'N-14°30'N, *Nature, 322,* 422-429, 1986.

Lockwood, J. P., J. J. Dvorak, T. T. English, R. Y. Koyanagi, A. T. Okamura, M. L. Summers, and W. R. Tanigawa, Mauna Loa 1974-1984; A decade of intrusive and extrusive activity, in *Volcanism in Hawaii*, edited by R. W. Decker, T. L. Wright and P. H. Stauffer, *U.S. Geol. Surv. Prof. Pap., 1350,* 537-570, 1987..

Lonsdale, P., Segmentation of the Pacific-Nazca spreading center, 1°N-20°S, *J. Geophys. Res., 94,* 12,197-12,226, 1989.

Macdonald, K. C., Linkages between faulting, volcanism, hydrothermal activity, and segmentation on fast spreading centers, in *Faulting and Magmatism at Mid-Ocean Ridges*, *Geophys. Monogr. Ser.*, vol. 106, edited by W. R. Buck, et al., pp. 27-58, AGU, Washington, D. C., 1998.

Macdonald, K. C., P. J. Fox, L. J. Perram, M. F. Eisen, R. M. Haymon, S. P. Miller, S. M. Carbotte, M.-H. Cormier, and A. N. Shor, A new view of the mid-ocean ridge from the behaviour of ridge axis discontinuities, *Nature, 335*, 217-225, 1988.

Macdonald, K. C., D. S. Scheirer, and S. M. Carbotte, Mid-ocean ridges: Discontinuties, segments and giant cracks, *Science, 253,* 986-994, 1991.

Macdonald, K. C., P. J. Fox, S. Carbotte, M. Eisen, S. Miller, L. Perram, D. Scheirer, S. Tighe, and C. Weiland, The East Pacific Rise and its flanks, 8°-18°N: History of segmentation, propagation and spreading direction based on SeaMARC II and Sea Beam studies, *Mar. Geophys. Res., 14*, 299-344, 1992.

Madsen, J. A., D. W. Forsyth, and R. S. Detrick, A new isostatic model for the East Pacific Rise crest, *J. Geophys. Res., 89*, 9997-10,015, 1984.

McClain, J. S., J. A. Orcutt, and M. Burnett, The East Pacific Rise in cross section: A seismic model, *J. Geophys. Res., 90*, 8627-8639, 1985.

MELT Seismic Team, Imaging the deep seismic structure beneath a mid-ocean ridge: The MELT experiment, *Science, 280,* 1215-1218, 1998.

Miller, T. P., R. G. McGimsey, D. H. Richter, J. R. Riehle, C. J. Nye, M. E. Yount, and J. A. Dumoulin, Catalog of Historically Active Volcanoes of Alaska, *U. S. Geol. Surv. Open File Rep. 98-582,* 104 pp., 1998.

Moore, J. G., Mechanism of formation of pillow lava, *Am. Sci., 63*, 269-277, 1975.

Neumann van Padang, M., *Catalog of Active Volcanoes of the World*, Int. Assoc. Volcanol. Chem. Earth Interior, Rome, 1951.

O'Neill, J. M. H., Geologic controls on distribution of hydrothermal vents on the superfast-spreading southern East Pacific Rise, M. A. thesis, 69 pp., Univ. of Calif. Santa Barbara, 1998.

Perfit, M. R., and W. W. Chadwick, Magmatism at mid-ocean ridges: Constraints from volcanological and geochemical investigations, in *Faulting and Magmatism at Mid-Ocean Ridges, Geophys. Monogr. Ser*., vol. 106, edited by W. R. Buck, et al., pp. 59-116, AGU, Washington, D. C., 1998.

Perfit, M. R., D. J. Fornari, M. C. Smith, J. F. Bender, C. H. Langmuir, and R. M. Haymon, Small-scale spatial and temporal variations in mid-ocean ridge crest magmatic processes, *Geology, 22,* 375-379, 1994.

Peterson, D. W., R. T. Holcomb, R. I. Tilling, and R. L. Christiansen, Development of lava tubes in the light of observations at Mauna Ulu, Kilauea Volcano, Hawaii, *Bull. Volcanol., 56,* 343-360, 1994.

Renard, V., R. Hekinian, J. Francheteau, R. D. Ballard, and H. Backer, Submersible observations at the axis of the ultra fast spreading East Pacific Rise (17°30' to 21°30'S), *Earth Planet. Sci. Lett., 88,* 339-353, 1985.

Reynolds, J. R., C. H. Langmuir, J. F. Bender, K. A. Kasten, and W. B. F. Ryan, Spatial and temporal variability in the geochemistry of basalts from the East Pacific Rise, *Nature, 359,* 493-499, 1992.

Rohr, K.M.M., B. Milkereit, and C.J. Yorath, Asymmetric deep crustal structure across the Juan de Fuca Ridge, *Geology, 16,* 533-537, 1988.

Rossi, M. J., Morphology and mechanism of eruption of postglacial shield volcanoes in Iceland, *Bull. Volcanol., 57,* 530-540, 1996.

Rubin, A. M., and D. D. Pollard, Origins of blade-like dikes in volcanic rift zones, in *Volcanism in Hawaii*, edited by R. W. Decker, T. L. Wright, and P. H. Stauffer, *U. S. Geol. Surv. Prof. Pap. 1350,* 1449-1470, 1987.

Scheirer, D. S., K. C. Macdonald, D. W. Forsyth, S. P. Miller, D. W. Wright, and M.-H. Cormier, A map series of the southern East Pacific Rise and it's flanks, 15°S to 19°S, *Mar. Geophys. Res., 18,* 1-12, 1996a.

Scheirer, D. S., K. C. Macdonald, D. W. Forsyth, and Y. Shen, Abundant seamounts of the Rano Rahi seamount field near the southern East Pacific Rise, 15º to 19ºS, *Mar. Geophys .Res., 18,* 13-52, 1996b.

Scheirer, D. S., D. W. Forsyth, M.-H. Cormier, and K. C. Macdonald, Shipboard geophysical indications of asymmetry and melt production beneath the East Pacific Rise near the MELT experiment,, *Science, 280,* 1221-1224, 1998.

Sempere, J.-C., J. R. Cochran, and S. S. Team, The Southeast Indian Ridge between 88°E and 118°E: Variations in crustal accretion at constant spreading rate, *J. Geophys. Res., 102,* 15,489-15,506, 1997.

Sigurdsson, H., Dyke injection in Iceland: A review, in *Mafic Dyke Swarms*, edited by H. C. Halls and W. F. Farig, *Geol. Assoc. Can. Spec. Pap. 34,* 55-64,1987.

Sigurdsson H. C., and S. R. J. Sparks, Lateral magma flow within rifted Icelandic crust, *Nature, 274*, 126-130, 1978.

Simkin, T., and L. Siebert, Earth's volcanoes and eruptions: An overview, in *Encyclopedia of Volcanoes*, edited by H. Sigmundsson, pp. 249-262, Academic, San Diego, Calif., 2000.

Singh, S. C., G. M. Kent, J. S. Collier, A. J. Harding, and J. A. Orcutt, Melt to mush variations in crustal magma properties along the ridge crest at the southern East Pacific Rise, *Nature, 394*, 874-878, 1998.

Sinton, J. M., S. M. Smaglik, J. J. Mahoney, and K. C. Macdonald, Magmatic processes at superfast spreading mid-ocean ridges: Glass compositional variations along the East Pacific Rise 13°-23°S, *J. Geophys. Res., 96*, 6133-6155, 1991.

Sinton, J. M., et al., Volcanic eruptions at superfast spreading mid-ocean ridges: Lava flows on the East Pacific Rise, 17-19°S, *Eos Trans. AGU, 80*(46), Fall Meet. Suppl., F1097, 1999.

Smellie, J. R., I. L. Millar, D. C. Rex, and P. J. Butterworth, Subaqueous, basaltic lava dome and carapace breccia on King George Island, South Shetland Islands, Antarctica, *Bull. Volcanol., 59*, 245-261, 1998.

Smith, D. K., and J. R. Cann, Constructing the upper crust of the Mid-Atlantic Ridge: A reinterpretation based on the Puna Ridge, Kilauea Volcano, *J. Geophys. Res., 104*, 25,379-25,400, 1999.

Smith, D. K., M. A. Tivey, H. Schouten, and J. R. Cann, Locating the spreading axis along 80 km of the Mid-Atlantic Ridge south of the Atlantis Transform, *J. Geophys. Res., 104*, 7599-7612, 1999.

Spudich, P. and J. A. Orcutt, A new look at the seismic velocity structure of the oceanic crust, *Rev. Geophys., 18*, 627-645, 1980.

Thorarinsson, S., The Lakagigar eruption of 1783, *Bull. Volcanol., 33*, 910-927, 1969.

Thorarinsson, S., and G. E. Sigvaldason, The Helka eruption of 1970, *Bull. Volcanol., 36*, 1-20, 1972.

Tribble, G. W., Underwater observations of active lava flows from Kilauea volcano, Hawaii, *Geology, 19*, 633-636, 1991.

Turcotte, D. L., and G. Schubert, *Geodynamics Applications of Continuum Physics to Geological Problems*, 450 pp., John Wiley, New York, 1982.

U. S. Geological Survey Juan de Fuca Study Group, Submarine fissure eruptions and hydrothermal vents on the southern Juan de Fuca Ridge: Preliminary observations from the submersible Alvin, *Geology, 14*, 823-827, 1986.

Walker, G. P. L., Structure, and origin by injection of lava under surface crust, of tumuli, "lava rises", "lava-rise pits", and "lava-inflation clefts" in Hawaii, *Bull. Volcanol., 53*, 546-558, 1991.

Walker, G. P. L., Basaltic volcanoes and volcanic systems, in *Encyclopedia of Volcanoes*, edited by H. Sigmundsson, pp. 283-289, Academic, San Diego, Calif., 2000.

White, S. M., K. C. Macdonald, D. S. Scheirer, and M.-H. Cormier, Distribution of isolated near-axis volcanoes on the flanks of the SEPR, 15.3°-20°S, *J. Geophys. Res., 103,* 30,371-30,384, 1998.

White, S. M., R. M. Haymon, D. J. Fornari, and K. C. Macdonald, Volcanic segmentation of the East Pacific Rise at 9°-10°N: evidence for high effusion-rate eruptions at segment center and low effusion-rate eruptions at segment ends (abstract), *Eos Trans. AGU,* in press, 2000.

Williams, H., The history and character of volcanic domes, *Bull. Dep. Geol. Sci. Univ. Calif. Publ., 21*, 51-146, 1932.

Wilson, D. S., Fastest known spreading on the Miocene Cocos-Pacific plate boundary, *Geophys. Res. Lett., 23*, 3003-3006, 1996.

Wolfe, E. W. (Ed)., *The Pu'u 'O'o eruption of Kilauea Volcano, Hawaii: Episodes 1 through 20, January 3, 1983, Through June 8, 1984*, *U. S. Geol. Surv. Prof. Pap. 1463*, 251 pp., 1988.

Wright, D. J., R. M. Haymon, and D. Fornari, Crustal fissuring and its relationship to magmatic and hydrothermal processes on the East Pacific Rise crest (9º12' to 54'N), *J. Geophys. Res., 100*, 6097-6120, 1995.

Wylie, J. J., K. R. Helfrich, B. Dade, J. R. Lister, and J. F. Salzig, Flow localization in fissure eruptions, *Bull. Volcanol., 60,* 432-440, 1999.

Figure Captions

Figure 1. Bathymetry of the axial high of the southern East Pacific Rise from a SeaBeam2000 survey in 1996 [*Cormier et al.*, 1996; *Scheirer et al.*, 1998]. The data were gridded at 100 m then plotted with a contour interval of 50 m and false illuminated from the northwest. (a) Dashed thick line follows the ridge axis. Solid bold line is the DSL-120 track. The locations of the topographic profiles in Figure 2 are labeled for reference. Inset map shows the location of the survey area with respect to the major plates. Inset diagram shows the minimum depth along the ridge axis of the East Pacific Rise. (b) Locations of the lava domes plotted as open circles and the third-order axial discontinuities from Table 2, which are bracketed (to the left) to show the length of ridge apparently disturbed by the discontinuity. Open circles are not scaled to the size of the lava domes. Magmatic segments identified by *Sinton et al.* [1991] on the basis of geochemical variation in ~10 km spaced dredge sampling are shown as I, J, and K.

Figure 2. Bathymetric profiles plotted along lines of constant latitude across the axial high from SeaBeam2000 data gridded at 100 m. Vertical exaggeration is 5:1. Arrows indicate the location of the ridge axis. The lines below the profile indicate the inferred position of graben-bounding faults. From top to bottom, the ridge axis lies (a) on the crest of a smooth dome, (b) in a half trough west of a scarp, (c) in a broad, shallow trough, and (d) in a deep, narrow trough. These four axial morphologies represent the four most common morphologies of fast-spreading ridges.

Figure 3. (left) Sidescan reflectance image from DSL-120 of Aldo Lake trough, and (right) geologic interpretation. Side-scan reflectance shows higher backscatter reflectivity as darker areas. The right panel shows a line drawing interpretation of the geology based on DSL-120 bathymetry gridded at 5 m and *Argo II* video coverage. The major collapses are outlined in solid black lines and represent individual lava lakes. The lava lakes are arranged en echelon, implying they formed over en echelon eruptive fissures. The areas of light gray fill are either lava sheet flows or collapsed lava tubes. Approximate locations of flow fronts and lava deltas at the ends of the tubes are shown with a dashed line.

Figure 4. (left) Side-scan reflectance image and (right) geologic interpretation of Pisco trough. Darker areas in the side-scan have higher backscatter reflectivity. The symbols used in the left panel are same as Figure 3, with the exception of two axial lava domes, shown in light gray fill with “D” on the right panel. The domes are differentiated from flow fronts by having a quasi-circular base, a strong (dark) acoustic backscatter reflection on their side nearest the sonar vehicle, a corresponding

weak (light) reflection on their far side, and positive relief of >10 m. Low-relief flow fronts appear to abut the base of the domes. Because these domes are slightly off axis, and apparently preexist the flows emanating from the collapse, either temporal variations in eruption style on axis, or the eruption of small off-axis dikes probably caused these domes to form.

Figure 5. DSL-120 side-scan phase bathymetry of the southern part of the Aldo Lake trough contoured at 2 m intervals. Closed contours are labeled "L" for local lows and "H" for highs. Lava tubes, 3-6 m deep, emanate from the 10-12 m deep collapsed lava lake. At the downslope end of the tube, the flow front of the lava delta is 6-8 m high. The floors of the collapsed lava tubes nearly on level with the floor of the lava lake collapses, and the nearly uniform height of the walls of the collapsed lake suggest that the entire structure may have formed in a single eruption.

Figure 6. An example of axial lava domes found at the end of a third-order ridge segment. Left panel shows the DSL-120 side-scan reflectance image from data gridded at 2 m. Darker areas in the side-scan have higher backscatter reflectivity. On the right panel, the DSL-120 phase bathymetry, gridded at 5 m, has been contoured at 5 m intervals. Black outlines show the digitized boundaries of the domes. Large fissures are continuous through several domes.

Figure 7. Sidescan reflectance image (left panel) and lava morphology map (right panel) of an area where good coverage of several domes was obtained with *Argo II*. Darker areas in the sidescan have higher backscatter reflectivity. We reviewed down-looking color video from several close-spaced *Argo II* lines, focusing on the classification of lava morphology, to make the lava morphology map. The lava flow morphology consists mainly of pillows (bulbous to quasi-spherical, breadcrust cracking, striations, and glassy buds) with some transitional pillow-lobate flows (somewhat bulbous, some breadcrust cracking, and few buds), and occasional lobate flows (slightly bulbous to flat, no breadcrust cracking, no buds). Lobate flows were observed at the summit of several domes. The sides of the domes are almost exclusively pillow lava; no sheet lava flows were observed.

Figure 8. Plot of the height and radius for each of the domes picked in this study. The radius of a dome was calculated as its basal perimeter divided by 2π for all of the axial lava domes imaged with >50% DSL-120 bathymetric coverage. Error bars show the ability of our DSL-120 side-scan bathymetry to measure the height to within 4m, and a 10% error on our ability to measure radii. The lines show the least squares linear regression best fit line to height:radius ratios from Icelandic lava shields (h=0.038r)[*Rossi*, 1996]. The stars indicate the sizes of documented small basaltic lava domes, labeled as follows: LH,

estimated size of Low Head on King George Island in Antarctica [*Smellie et al.*, 1998]; KEJ, 1978 dome formed on Kick'em-Jenny [*Devine and Sigurdsson*, 1995]; B, Bogoslof eruption of 1927 in the Aleutian Islands [*Miller et al.*, 1998]; MC, Mamelon Central dome formed in 1791 on Reunion Island that subsequently collapsed [*Neumann van Padang*, 1951]. These examples are all of the small basaltic lava domes known to us, and all lie near the center of the field defined by the southern East Pacific Rise (SEPR) axial domes.

Figure 9. Histograms of the cumulative number of axial lava domes for each of three possible orders of segmentation in the survey area. Bin interval is normalized to represent 20% of the distance from segment end to midsegment in order to adjust for segments of varying length. (a) When only overlapping spreading centers (OSCs) are considered, a bimodal trend to the histogram distribution of axial lava domes implies a finer order of segmentation bisects most of the OSC-bounded segments. (b) The decreasing trend from segment end to the center of the number of axial volcanic mounds is observed only when all of the third-order segments are considered. (c) On the very fine scale fourth-order segments identified from the DSL-120 maps, no systematic distribution of lava domes is observed.

Figure 10. The mean basal area of the axial lava domes shows a general decrease away from third-order segment ends. Bin interval is normalized to include 20% of the third-order segment length (same as Figure 9).

Figure 11. The lava morphology for the three northernmost third-order segments of this survey where dense *Argo II* coverage is available follows the pattern expected from the observations of pillow lava domes using DSL-120 sonar. To obtain the percentage of each lava morphology, the total area covered by the lava morphology was statistically determined, as described in the text, then divided by the total area visually imaged in each bin interval by 1996 *Argo II* survey. Bin interval is normalized to include 20% of the third-order segment length (same as Figure 9), and bins are mirrored around the segment center. The major volcanic structures seen on the ridge crest (drawn schematically on bottom panel) reflect changes in the dominant lava morphology observed. Using lava morphology as an indicator of effusion rate suggests that effusion rate drops off systematically toward the ends of third-order (volcanic) ridge segments.

Figure 12. Along-axis comparison of ridge structure to the location of volcanic (third-order) ridge segments. First panel shows depth of the ridge axis, from SeaBeam 2000 bathymetry [*Cormier et al.*, 1996], with ±10m error bars. Second panel shows two-way travel time to seismic layer 2A, and third panel shows two-way travel time to axial magma chamber (AMC) reflector, both panels with ±0.003s error bars [*Detrick et al.*, 1993]. Fourth panel is a histogram of the abundance of axial pillow domes binned at 2 minute (~3.7 km) interval. Locations of the volcanic (third-order) ridge discontinuity zones are shown with a light gray bar to show the length of the ridge apparently disturbed by the discontinuity as in Figure 1b. Segment ends correlate with lava domes and with AMC depth to some degree, but there is no clear correlation with axial depth or layer 2A thickness.

Figure 13. The distribution of axial lava domes at the northernmost third-order ridge segment in our study area. SeaBeam 2000 bathymetry of the axial high of the southern East Pacific Rise presented as in Figure 1 but without contour lines. Black lines outline the base of each axial lava dome picked from the DSL-120 data, and the location of the Aldo Lake trough is shown in gray fill. Dashed lines show the width of the zone of layer 2A accumulation as determined by *Carbotte et al.* [1997], and thick solid lines just below show the width of the AMC [*Hooft et al.*, 1997] at the locations of across-axis seismic lines. Aldo Lake trough, the inferred volcanic center of the segment, extends southward from the geographical segment center. Axial pillow lava domes occur throughout the segment and are most abundant around the segment offsets (shown within brackets as in Figure 1b).

Table 1. Characteristics of Segmentation Updated From *Macdonald et al.* [1991].

Segments	Order 1	Order 2	Order 3	Order 4
Segment length, km	600 ± 300	140 ± 90	20 ± 10 [a]	7 ± 5 [a]
Segment longevity, years	> 5 x 10^6	0.5 - 5 x 10^6	~10^4 - 10^5	< 10^3 [a]
Discontinuities	**Order 1**	**Order 2**	**Order 3**	**Order 4**
Type	transform, large propagating rifts	overlapping spreading centers (oblique shear zones, rift valley jogs)	Overlapping Spreading Centers, DevALs, Saddle Points[a] (intervolcano gaps)	DevALs, offsets of axial summit caldera or fissure systems[a] (intravolcano gaps)
Offset, km	> 30 km	1-30 km	0 - 1 km[a]	< 0.2 km[a]
Depth anomaly	300-600 m	100-300 m	30-100 m[a]	0-30 m[a]
Off-axis trace	fracture zone	V shaped discordant zone	faint or none	none

a. Changes based on detailed observations of SEPR

Table 2. Third-Order Ridge Axis Discontinuities, Location and Description.

Latitude	Longitude	Structure/Morphology	Length, km
17° 11’ S	113° 8.5’ W	start of survey, midsegment	
17° 18.5’ S	113° 10.6’ W	saddle point	14.7
17° 30’ S	113° 13.5’ W	left-stepping non-overlapping offset	22
17° 35.75’ S	113° 15’ W	left-stepping non-overlapping offset	11
17° 40’ S	113° 15.75’ W	saddle point	8.1
17° 56’ S	113° 17.75’ W	left-stepping overlapping spreading center	29.6
18° 02.5’ S	113° 19’ W	left-stepping non-overlapping offset	12.3
18° 09’ S	113° 20.75’ W	left-stepping overlapping offset at transition between half-graben and full-graben ridge axis	12.4
18° 22’ S	113° 22’ W	left-stepping overlapping spreading center	24.6
18° 30.75’ S	113° 24.7’ W	Left-stepping non-overlapping offset	18.5
18° 33.5’ S	113° 25.25’ W	end of survey, north of overlapping spreading center	

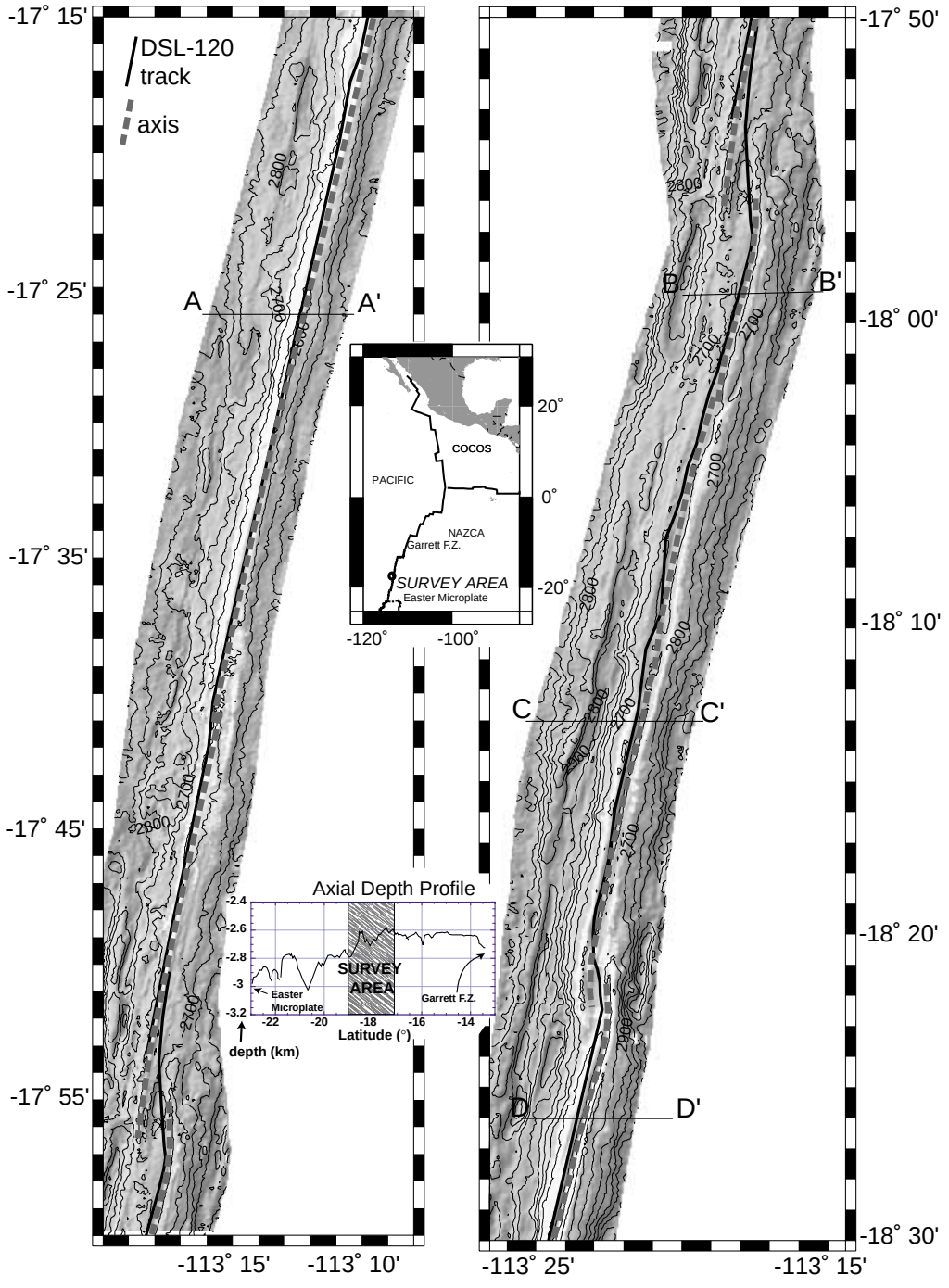
-17° 15'
-17° 25'
-17° 35'
-17° 45'
-17° 55'
-113° 15'
-113° 10'
-113° 25'
-113° 15'
-17° 50'
-18° 00'
-18° 10'
-18° 20'
-18° 30'
DSL-120 track
axis
A
A'
B
B'
C
C'
D
D'
2800
2700
2600
COCOS
PACIFIC
NAZCA
Garrett F.Z.
SURVEY AREA
Easter Microplate
20°
0°
-20°
-120°
-100°
Axial Depth Profile
SURVEY AREA
Easter Microplate
Garrett F.Z.
depth (km)
Latitude (°)

a.

Figure 1a

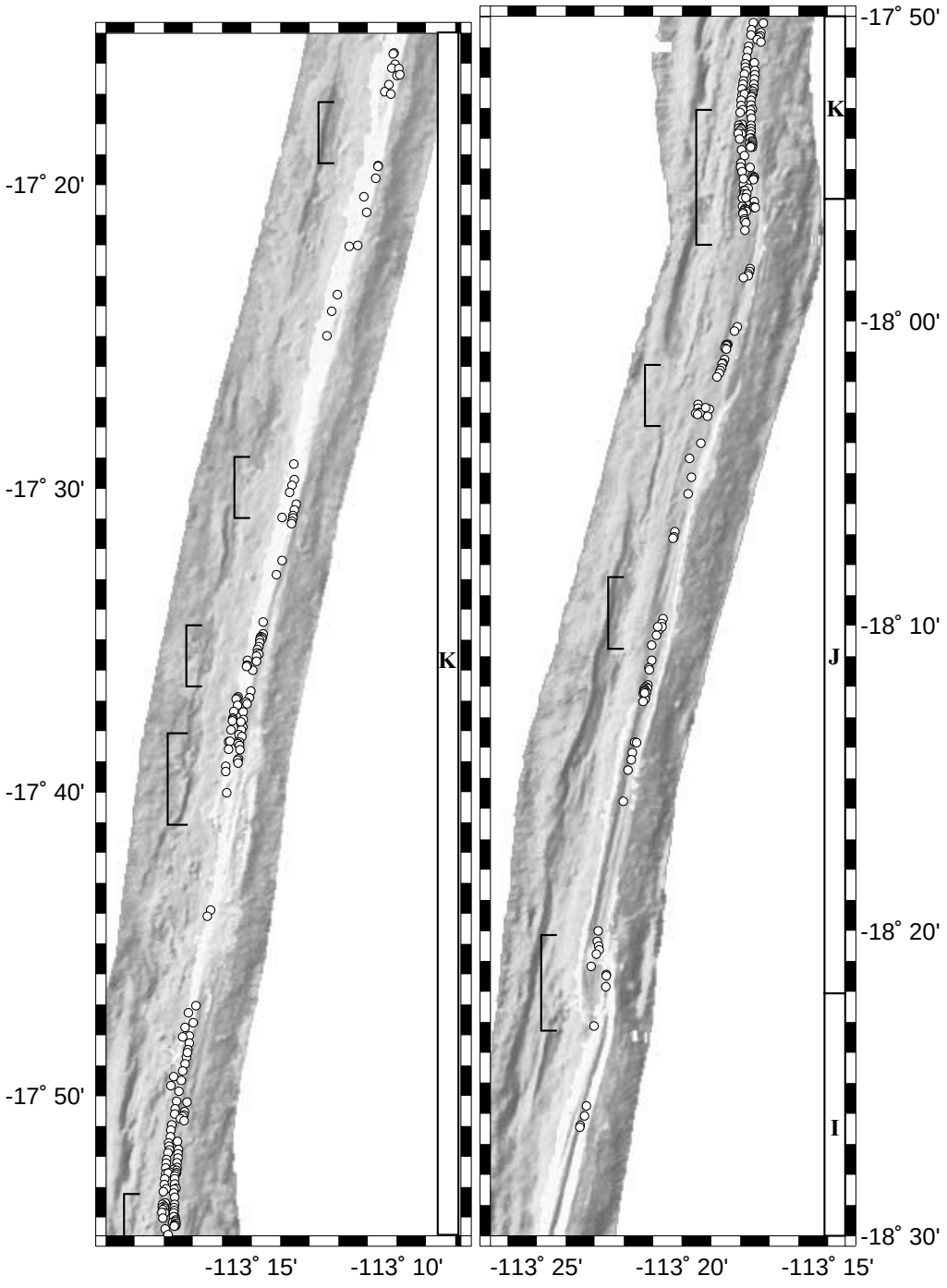
-17˚ 20'
-17˚ 30'
-17˚ 40'
-17˚ 50'
-113˚ 15'
-113˚ 10'
-113˚ 25'
-113˚ 20'
-113˚ 15'
-17˚ 50'
-18˚ 00'
-18˚ 10'
-18˚ 20'
-18˚ 30'
K
K
J
I

b.

Figure 1b

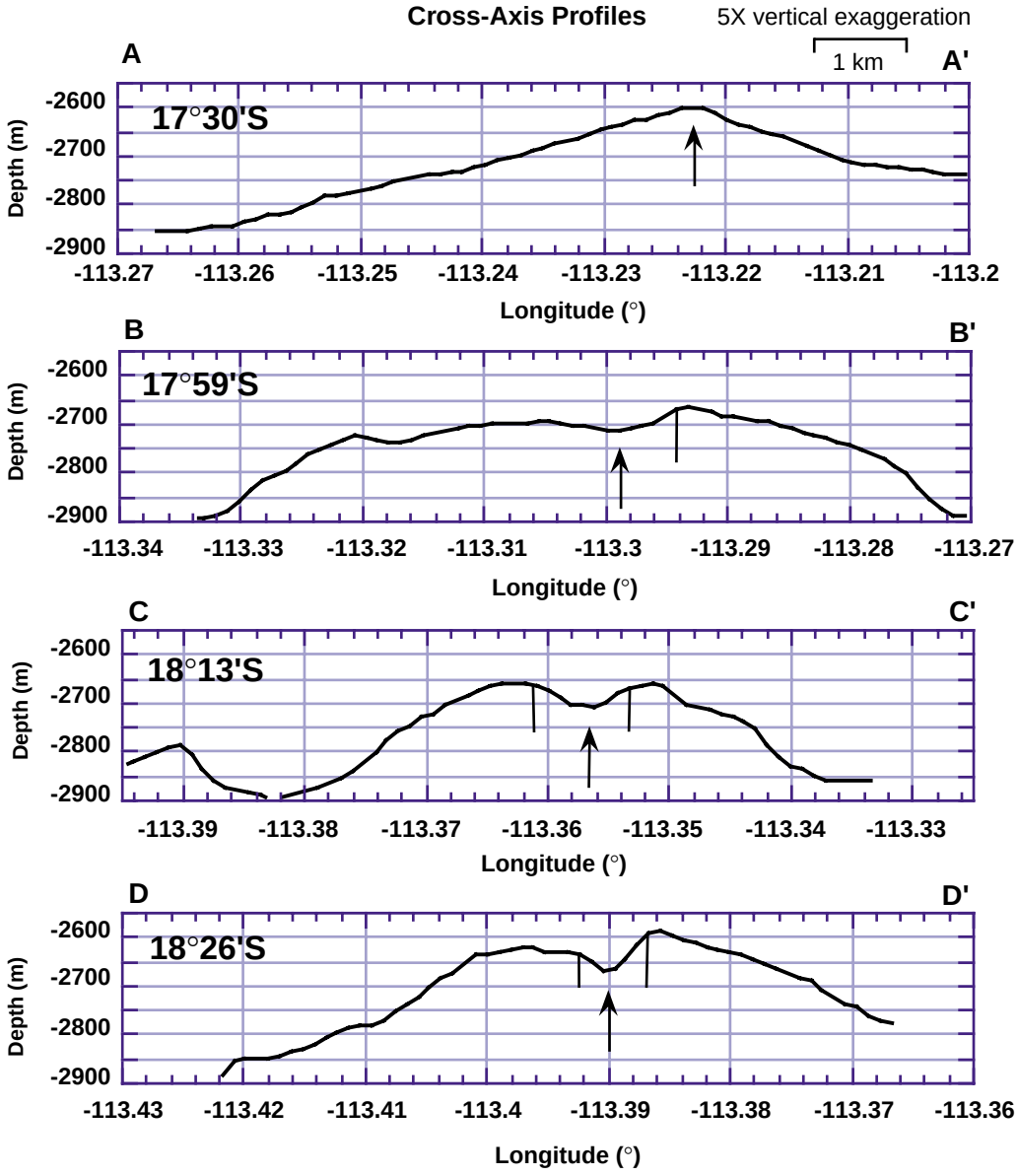
Cross-Axis Profiles
5X vertical exaggeration
1 km
A
A'
17°30'S
Depth (m)
-2600
-2700
-2800
-2900
-113.27
-113.26
-113.25
-113.24
-113.23
-113.22
-113.21
-113.2
Longitude (°)
B
B'
17°59'S
-113.34
-113.33
-113.32
-113.31
-113.3
-113.29
-113.28
-113.27
C
C'
18°13'S
-113.39
-113.38
-113.37
-113.36
-113.35
-113.34
-113.33
D
D'
18°26'S
-113.43
-113.42
-113.41
-113.4
-113.39
-113.38
-113.37
-113.36

Figure 2

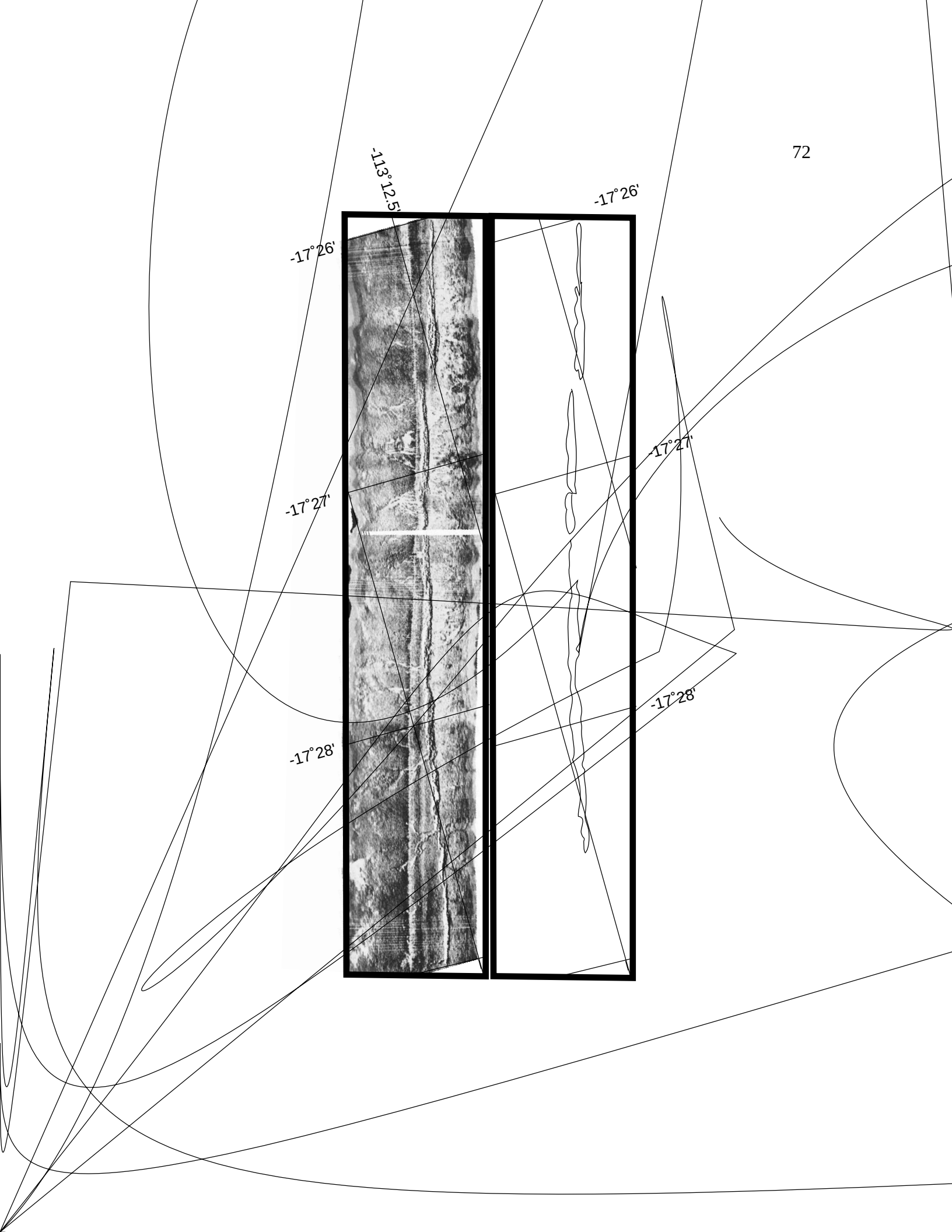
-113°12.5'
-17°26'
-17°26'
-17°27'
-17°27'
-17°28'
-17°28'

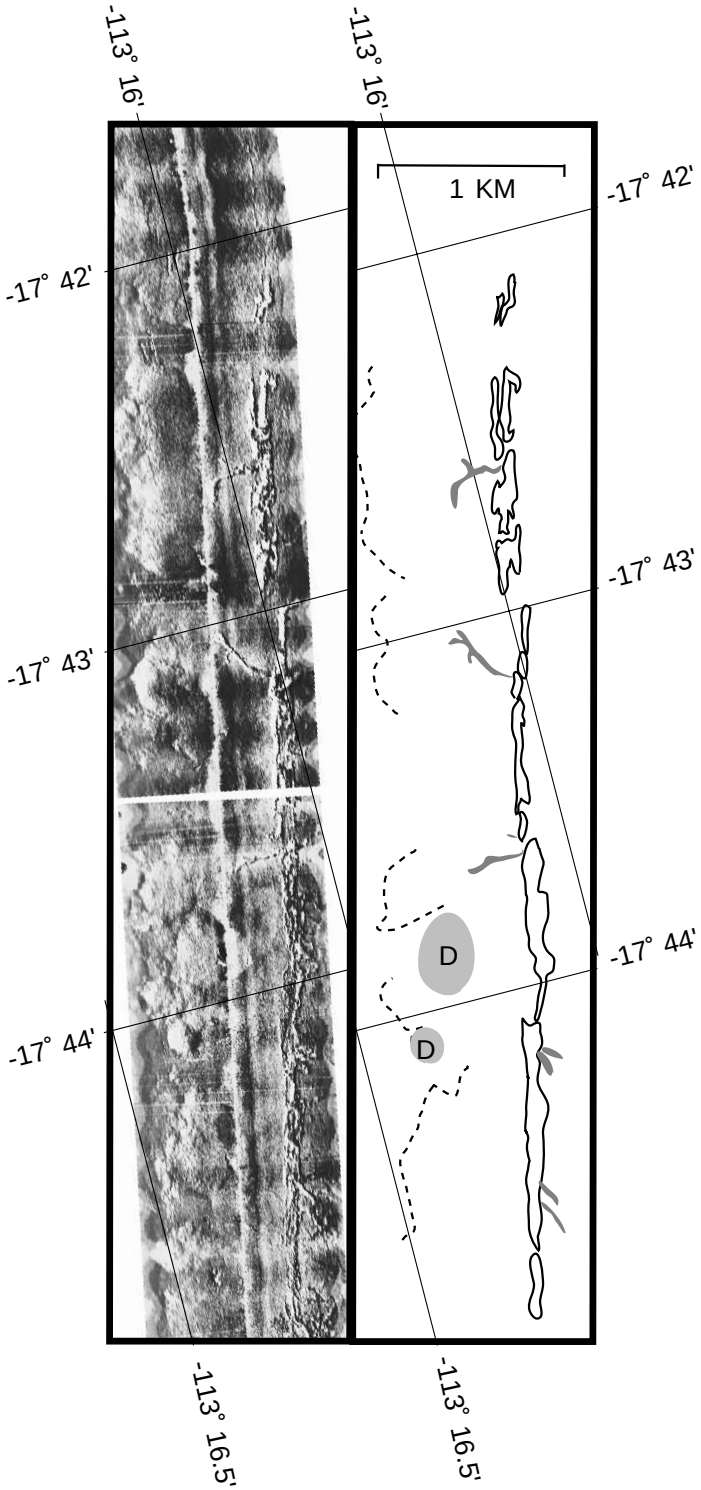
-113° 16'
-113° 16'
1 KM
-17° 42'
-17° 42'
-17° 43'
-17° 43'
D
-17° 44'
D
-17° 44'
-113° 16.5'
-113° 16.5'

Figure 4

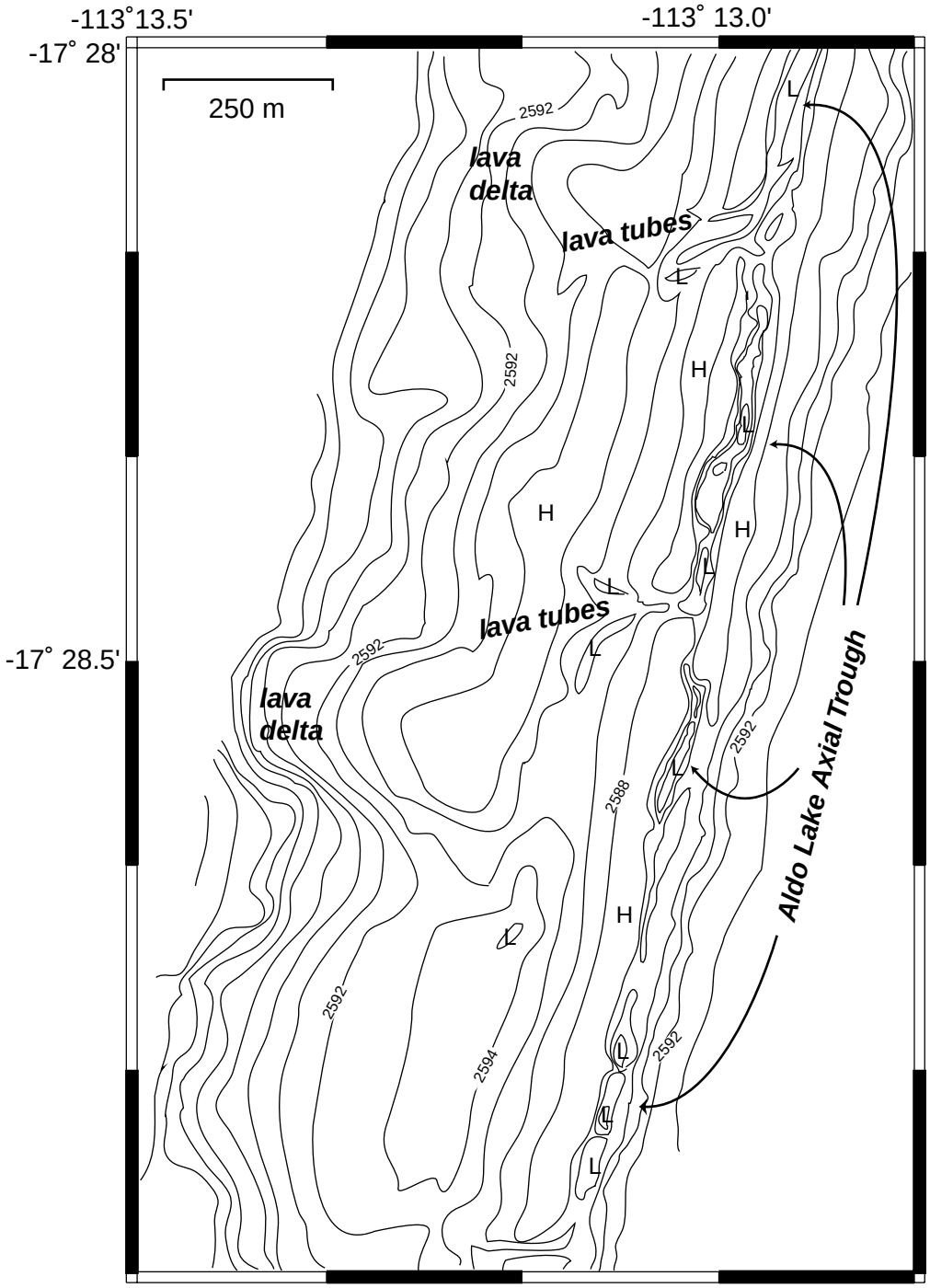
-113˚13.5'
-113˚ 13.0'
-17˚ 28'
-17˚ 28.5'
250 m
2592
lava
delta
lava tubes
H
L
2592
H
H
L
lava tubes
2592
lava
delta
2592
2588
Aldo Lake Axial Trough
H
2592
2594
2592
L

Figure 5

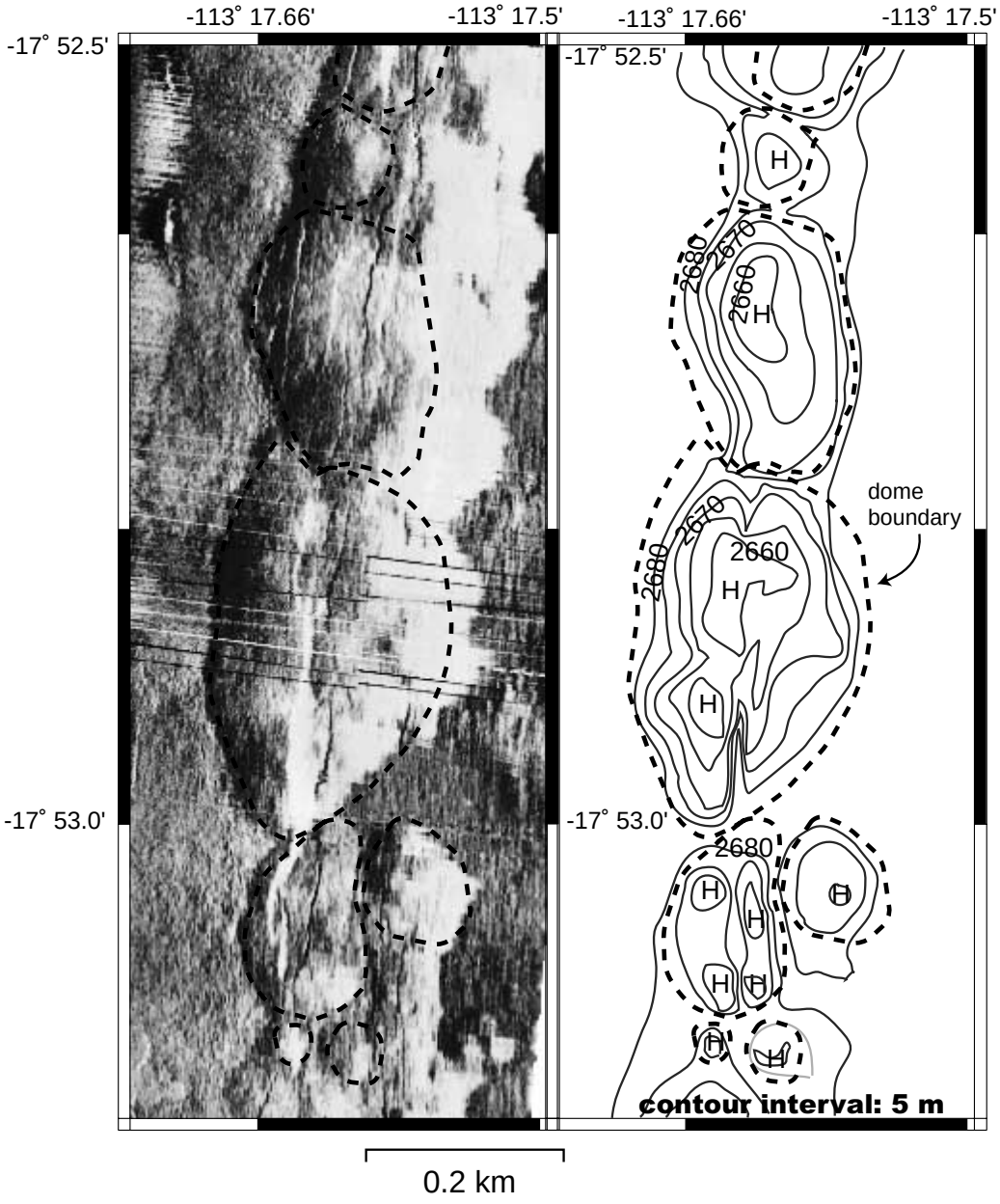
-113˚ 17.66'
-113˚ 17.5'
-17˚ 52.5'
-17˚ 53.0'
2680
2670
2660
H
dome
boundary
contour interval: 5 m
0.2 km

Figure 6

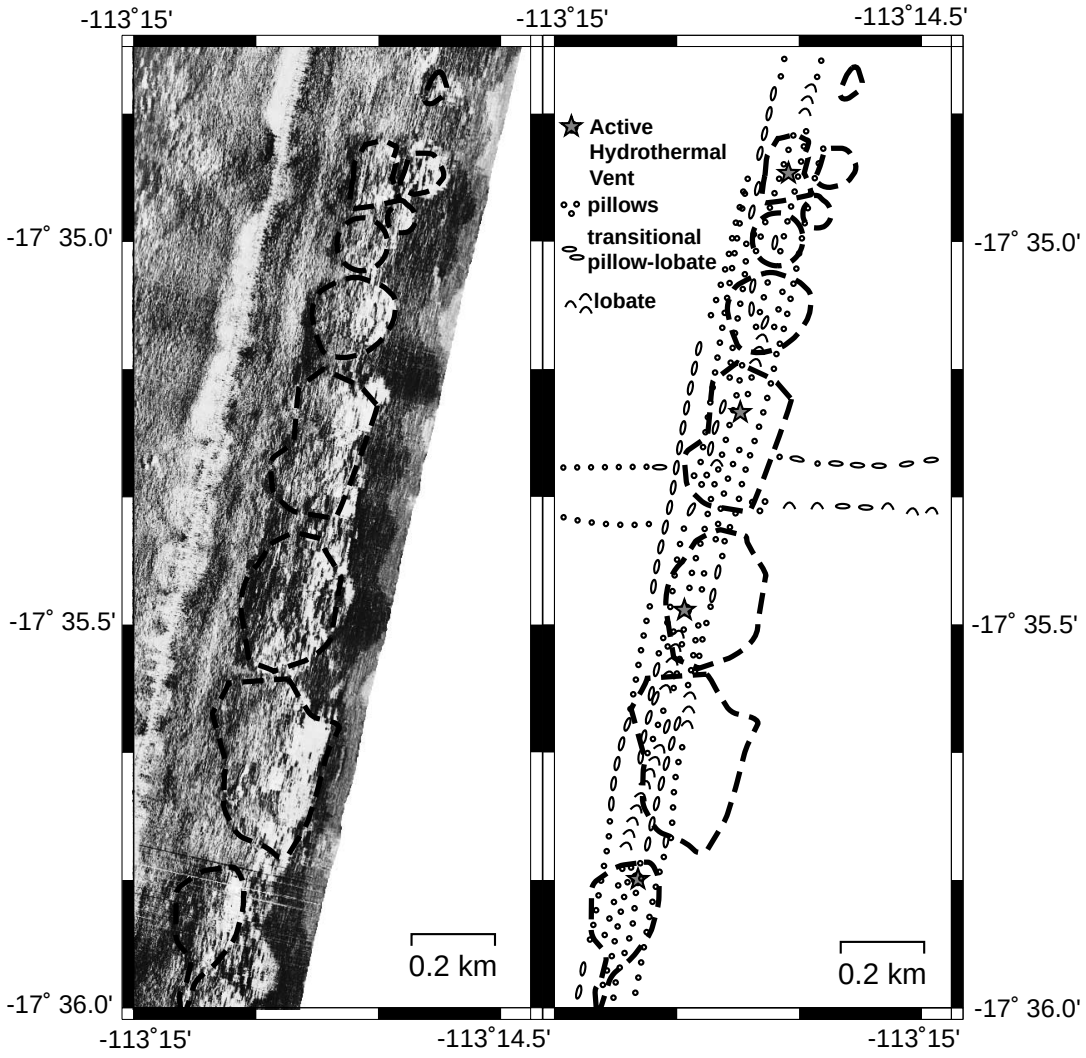
-113˚15'
-113˚15'
-113˚14.5'
-17˚ 35.0'
-17˚ 35.5'
-17˚ 36.0'
Active Hydrothermal Vent
pillows
transitional pillow-lobate
lobate
0.2 km
0.2 km
-113˚15'
-113˚14.5'
-113˚15'

Figure 7

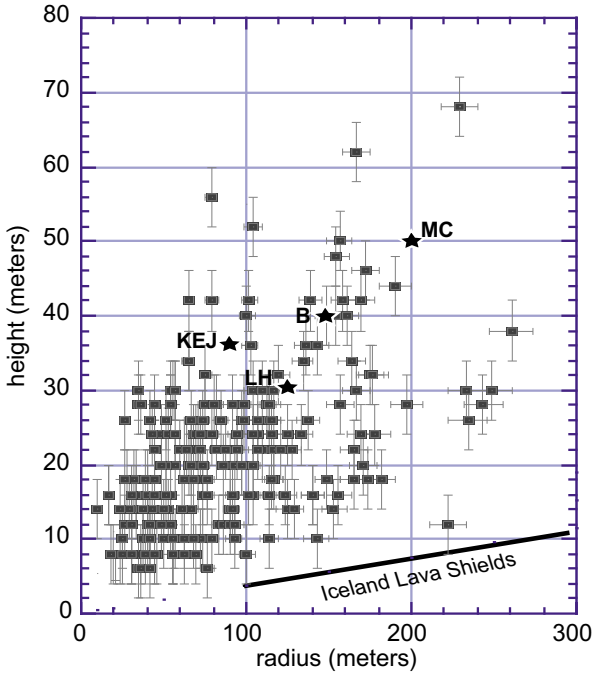
height (meters)
radius (meters)
0
10
20
30
40
50
60
70
80
0
100
200
300
MC
B
KEJ
LH
Iceland Lava Shields

Figure 8

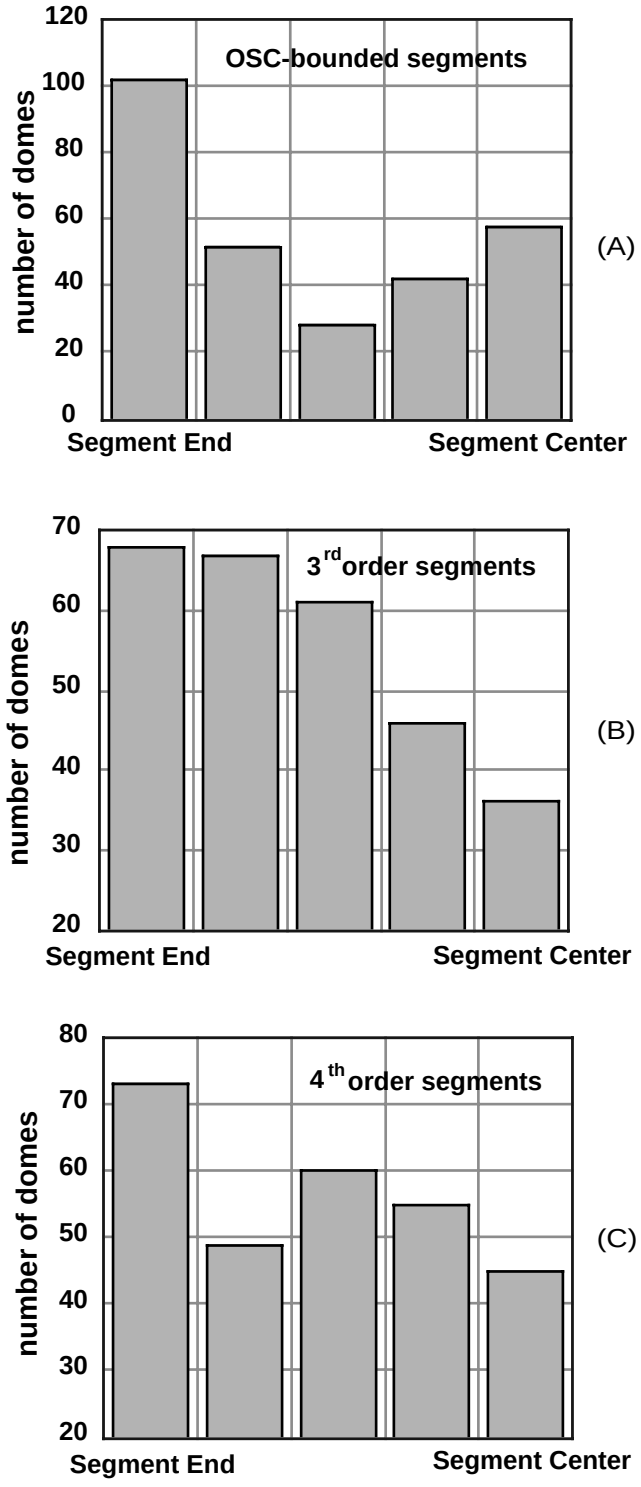
OSC-bounded segments
number of domes
120
100
80
60
40
20
0
Segment End
Segment Center
(A)
3rd order segments
number of domes
70
60
50
40
30
20
Segment End
Segment Center
(B)
4th order segments
number of domes
80
70
60
50
40
30
20
Segment End
Segment Center
(C)

Figure 9

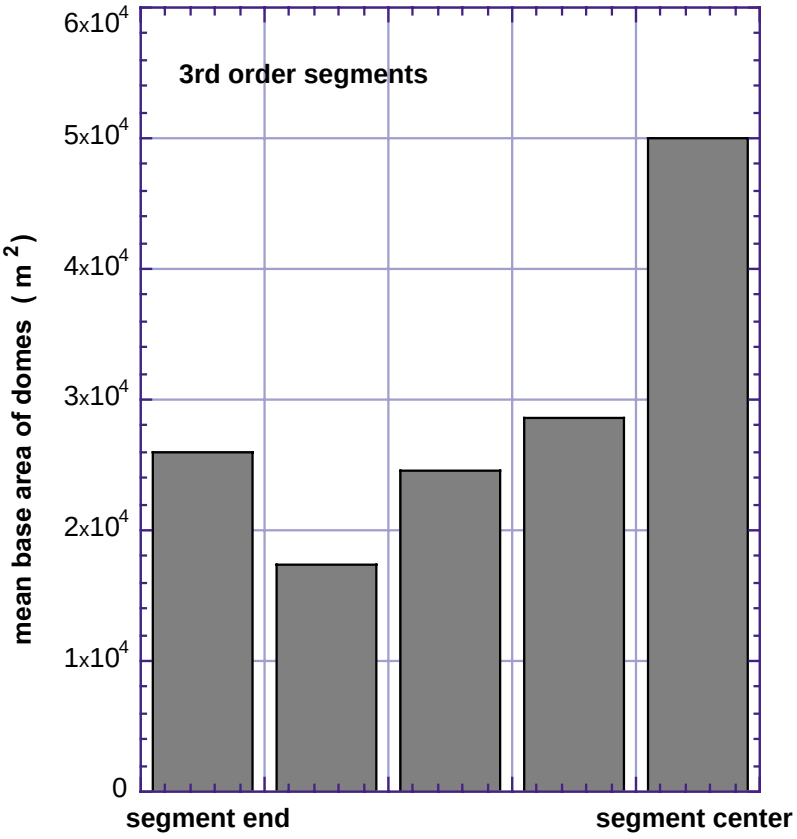
3rd order segments
mean base area of domes (m 2)
6x10^4
5x10^4
4x10^4
3x10^4
2x10^4
1x10^4
0
segment end
segment center

Figure 10

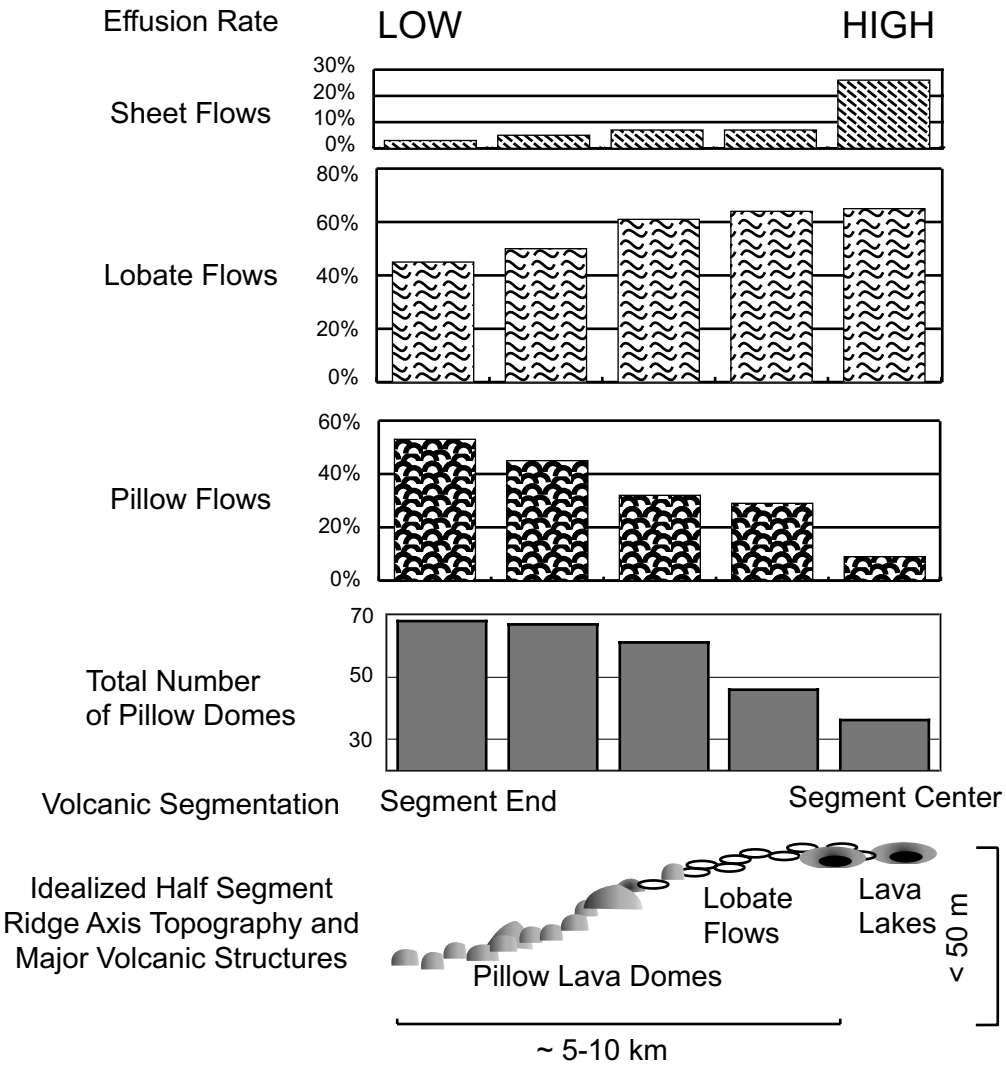
Effusion Rate
LOW
HIGH
Sheet Flows
30%
20%
10%
0%
Lobate Flows
80%
60%
40%
20%
0%
Pillow Flows
60%
40%
20%
0%
Total Number of Pillow Domes
70
50
30
Volcanic Segmentation
Segment End
Segment Center
Idealized Half Segment Ridge Axis Topography and Major Volcanic Structures
Lobate Flows
Lava Lakes
< 50 m
Pillow Lava Domes
~ 5-10 km

Figure 11

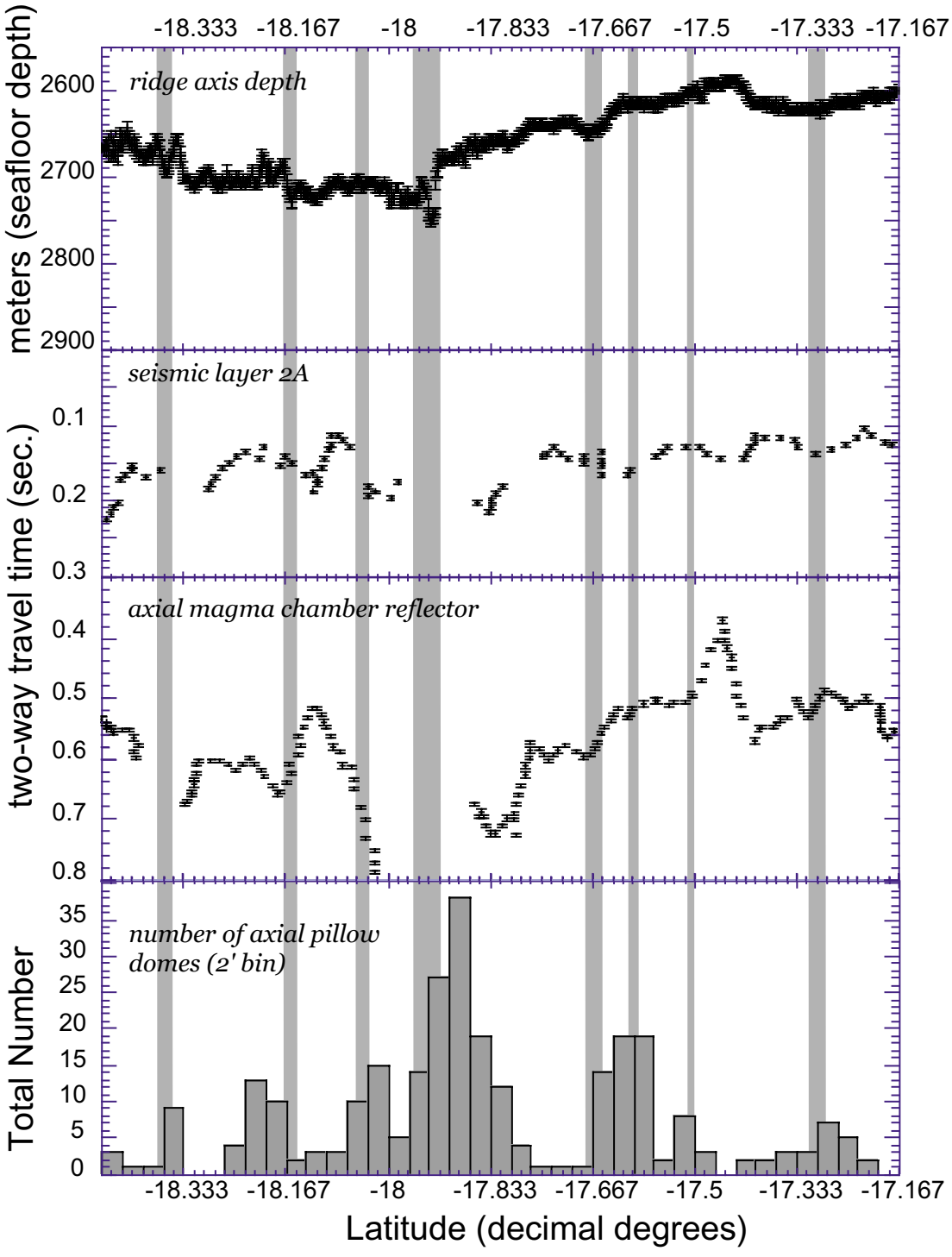
-18.333
-18.167
-18
-17.833
-17.667
-17.5
-17.333
-17.167
meters (seafloor depth)
2600
2700
2800
2900
ridge axis depth
seismic layer 2A
two-way travel time (sec.)
0.1
0.2
0.3
axial magma chamber reflector
0.4
0.5
0.6
0.7
0.8
Total Number
35
30
25
20
15
10
5
0
number of axial pillow domes (2' bin)
Latitude (decimal degrees)

Figure 12

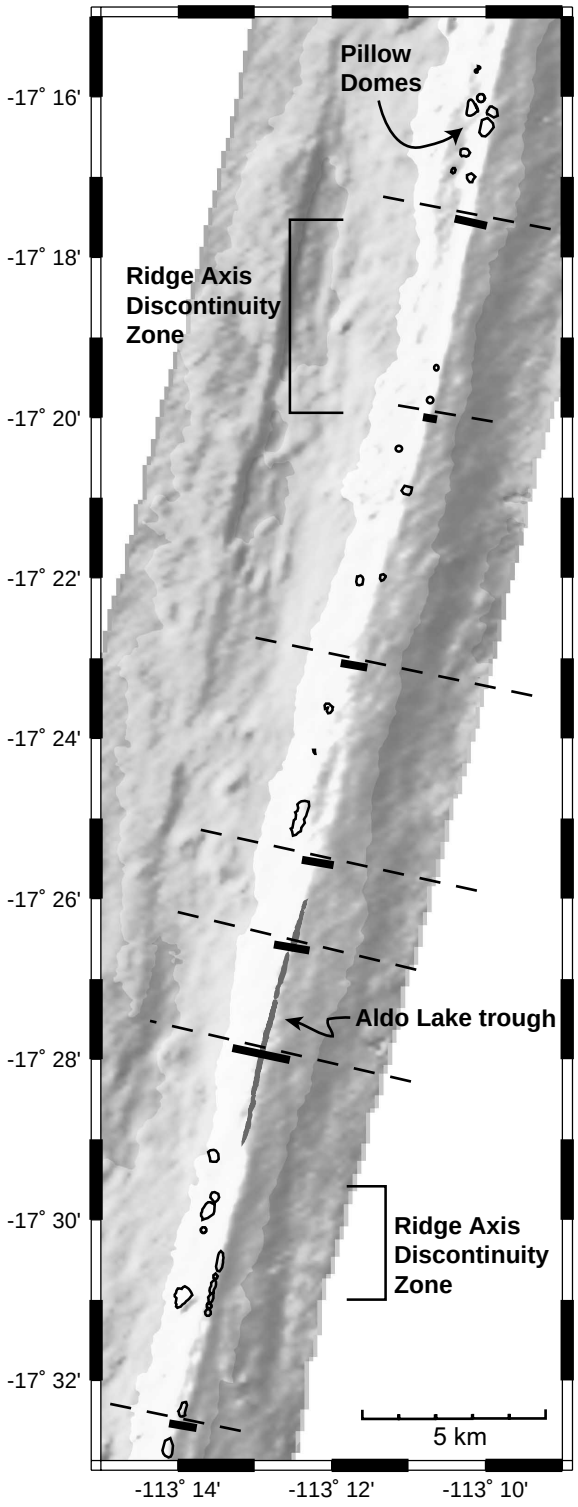
Pillow
Domes
Ridge Axis
Discontinuity
Zone
Aldo Lake trough
Ridge Axis
Discontinuity
Zone
5 km
-17° 16'
-17° 18'
-17° 20'
-17° 22'
-17° 24'
-17° 26'
-17° 28'
-17° 30'
-17° 32'
-113° 14'
-113° 12'
-113° 10'

Figure 13